



可充放锌空电池用过渡金属氧化物双功能催化剂研究进展

刘渐芳 赵勇智 王永 刘鸾 刘思佳 秦运璞 吴昊阳 张德印 贾宝瑞 曲选辉 秦明礼

Advancements in the study of transition metal oxide bifunctional catalysts for rechargeable zinc-air batteries

LIU Jianfang, ZHAO Yongzhi, WANG Yong, LIU Luan, LIU Sijia, QIN Yunpu, WU Haoyang, ZHANG Deyin, JIA Baorui, QU Xuanhui, QIN Mingli

引用本文:

刘渐芳, 赵勇智, 王永, 刘鸾, 刘思佳, 秦运璞, 吴昊阳, 张德印, 贾宝瑞, 曲选辉, 秦明礼. 可充放锌空电池用过渡金属氧化物双功能催化剂研究进展[J]. *工程科学学报*, 2024, 46(1): 56–72. doi: 10.13374/j.issn2095–9389.2023.03.14.001

LIU Jianfang, ZHAO Yongzhi, WANG Yong, LIU Luan, LIU Sijia, QIN Yunpu, WU Haoyang, ZHANG Deyin, JIA Baorui, QU Xuanhui, QIN Mingli. Advancements in the study of transition metal oxide bifunctional catalysts for rechargeable zincair batteries[J]. *Chinese Journal of Engineering*, 2024, 46(1): 56–72. doi: 10.13374/j.issn2095–9389.2023.03.14.001

在线阅读 View online: <https://doi.org/10.13374/j.issn2095–9389.2023.03.14.001>

您可能感兴趣的其他文章

Articles you may be interested in

基于过渡金属氧化物载氧体的煤矿通风瓦斯处理性能

Performance of ventilation air methane combustion over transition metal oxide oxygen carriers

工程科学学报. 2017, 39(6): 823 <https://doi.org/10.13374/j.issn2095–9389.2017.06.002>

钙钛矿型锂离子固体电解质 $\text{Li}_{2xy}\text{Sr}_{1x}\text{Ti}_{1y}\text{Nb}_y\text{O}_3$ 的性能

Performance of perovskite-type Li-ion solid electrolyte $\text{Li}_{2xy}\text{Sr}_{1x}\text{Ti}_{1y}\text{Nb}_y\text{O}_3$

工程科学学报. 2021, 43(8): 1024 <https://doi.org/10.13374/j.issn2095–9389.2020.12.03.004>

$\text{Ba}_3\text{Ca}_{1+x}\text{Nb}_{2x}\text{O}_{9\delta}$ 复合钙钛矿型固体电解质性能研究

Transport properties of $\text{Ba}_3\text{Ca}_{1+x}\text{Nb}_{2x}\text{O}_{9\delta}$ composite perovskite oxides

工程科学学报. 2021, 43(8): 1032 <https://doi.org/10.13374/j.issn2095–9389.2020.12.03.003>

一种高效双功能电催化剂CoP/Co@NPC@rGO的制备

Preparation of CoP/Co@NPC@rGO nanocomposites with an efficient bifunctional electrocatalyst for hydrogen evolution and oxygen evolution reaction

工程科学学报. 2020, 42(1): 91 <https://doi.org/10.13374/j.issn2095–9389.2019.07.26.002>

废催化剂中铂族金属回收现状与研究进展

Status and research progress on recovery of platinum group metals from spent catalysts

工程科学学报. 2020, 42(3): 257 <https://doi.org/10.13374/j.issn2095–9389.2019.11.26.001>

钙钛矿太阳能电池稳定性研究进展

Research progress on the stability of perovskite solar cells

工程科学学报. 2020, 42(1): 16 <https://doi.org/10.13374/j.issn2095–9389.2019.06.24.006>

可充放锌空电池用过渡金属氧化物双功能催化剂研究进展

刘渐芳, 赵勇智, 王永, 刘 鸾, 刘思佳, 秦运璞, 吴昊阳, 张德印, 贾宝瑞[✉], 曲选辉, 秦明礼[✉]

北京科技大学新材料技术研究院, 北京 100083

✉通信作者, 贾宝瑞, E-mail: jibaorui@ustb.edu.cn; 秦明礼, E-mail: qinml@mater.ustb.edu.cn

摘 要 近年来,可充放锌-空气二次电池因其高理论比能密度、高安全性、环境友好、低成本等优点,引起了广泛的关注,被认为是未来电网和电动汽车供电的可行选择之一。锌空电池中,氧还原反应和析氧反应催化剂的活性和稳定性对电池的能量密度、功率密度和寿命有重要影响,因此,开发高效、稳定的氧还原/析氧反应双功能催化剂已经成为一个重要研究方向。本文介绍了不同种类过渡金属氧化物催化剂的活性来源及其在锌空电池能量密度、充/放电电压、循环寿命等方面的表现,总结了当下研究现状中提高催化性能的策略和方法。

关键词 锌空电池; 电催化剂; 过渡金属氧化物; 尖晶石; 钙钛矿

分类号 O646

Advancements in the study of transition metal oxide bifunctional catalysts for rechargeable zinc-air batteries

LIU Jianfang, ZHAO Yongzhi, WANG Yong, LIU Luan, LIU Sijia, QIN Yunpu, WU Haoyang, ZHANG Deyin, JIA Baorui[✉], QU Xuanhui, QIN Mingli[✉]

Institute for Advanced Materials and Technology, University of Science and Technology Beijing, Beijing 100083, China

✉Corresponding authors, JIA Baorui, E-mail: jibaorui@ustb.edu.cn; QIN Mingli, E-mail: qinml@mater.ustb.edu.cn

ABSTRACT In recent years, rechargeable zinc-air batteries (ZABs) have attracted much attention owing to their high theoretical specific energy density, safety, and environmental friendliness. They are also considered a viable option for powering the grid and electric vehicles in the future. The activity and the stability of the bifunctional catalysts for the oxygen reduction reaction (ORR) and the oxygen evolution reaction (OER) in ZABs remarkably influence the battery's energy, power densities, and lifetime. Therefore, developing efficient and stable bifunctional catalysts is an important research direction. Previously, precious metal catalysts such as Pt/C, Ir/C, and Ru/C have been used to design efficient ORR and OER electrocatalysts. However, these electrocatalysts possess several issues, including limited natural abundance, high metal sintering and catalyst detachment rates from supports, and poor bifunctional activity, which limit their practical applications. As potential catalysts, nonprecious transition metal oxides exhibit the prominent advantages of manifold compositions, multiple valence states, environmental friendliness, high durability and abundance, and varying structures. Their disadvantages include poor electrical conductivity and a limited surface area. To address the abovementioned issues, current general research focuses on compounding transition metal oxides with carbon materials or other conductive substrates to simultaneously increase their specific surface area and electrical conductivity and control their morphology to expose more active sites. Furthermore, the intrinsic

收稿日期: 2023-05-23

基金项目: 国家重点研发计划资助项目(2022YFB3708800)

activity of the transition metal oxides must also be regulated through the most commonly used activity regulation methods (e.g., heteroatom doping and defect engineering). For example, perovskite and spinel-type transition metal oxides must meet a specific e_g orbital occupancy to achieve the best bifunctional activity. Therefore, improving the catalytic performance requires the A- and B-site atom substitution with other alkaline and rare earth or transition metals or the introduction of oxygen vacancies to adjust the electronic structure. Spinel- and perovskite-type transition metals and manganese oxides are the research objects used in this work. The activity sources of different types of transition metal oxide catalysts and their performances in energy density, charge/discharge voltage, and cycle life of zinc-air batteries are introduced herein. The strategies and methods used to improve the catalytic performance of transition metal oxides in current research are summarized. Finally, the future development of transition metal bifunctional catalysts for oxygen reduction and evolution reactions is prospected.

KEY WORDS zinc-air batteries; electrocatalyst; transition metal oxides; spinel; perovskite

近年来, 受现阶段严重的环境问题和日益增长的能源需求所带来的影响, 开发绿色、可持续的能量转换和存储技术已经发展成为现代社会的重大课题^[1-2]. 目前, 锂(Li)离子二次电池作为代表性电化学能源技术, 引领着储能市场, 尤其在电子消费品和混合动力/纯电动汽车领域占据着主流地位. 然而, 传统可充电二次锂离子电池容量一般在 200 ~ 250 W·h·kg⁻¹ 之间, 能量密度的不足部分限制了其进一步发展和应用^[3-5]. 金属-空气电池的理论能量密度比传统锂离子电池高数倍, 被认为是未来社会能源储存问题的有效解决方案之一, 受到越来越多的关注^[6-7]. 在各类金属-空气电池中金属负极的理论比容量(质量比能量密度)、体积比能量密度和电池电压的比较中, 锌-空气电池(Zinc-air batteries, ZABs)展现出优异的综合性能, 其具有高的质量比能量密度(1218 W·h·kg⁻¹)和体积比能量密度(6136 W·h·L⁻¹), 且锌储量丰富、价格低廉, 常采用水作为溶剂, 绿色环保、安全性高, 因而受到人们的广泛关注^[8-9].

ZABs 是一种以空气中的氧气作为正极电化学反应物质, 金属锌作为负极电化学反应物质的新型储能器件, 通常由四个主要部件组成^[10-11]: 空气电极(催化剂负载的气体扩散层)、碱性电解质、隔膜和锌电极. 放电时, 锌极发生氧化反应, 释放的电子通过外部电路到达空气电极. 同时, 大气中的氧分子在空气电极的三相界面处发生氧还原反应(Oxygen reduction reaction, ORR), 该反应产生的氢氧根离子迁移至锌电极, 形成锌酸根离子, 随后分解为不溶性氧化锌, 总反应的平衡电压为 1.66 V. ZABs 充电时, 化学反应与上述过程相反, 锌重新沉积在锌电极处, 氢氧根离子通过析氧反应(Oxygen evolution reaction, OER)于三相界面释放氧气. 其化学反应可简化为如下所示^[12]: 锌阳极, $Zn + 4OH^- \rightleftharpoons Zn(OH)_4^{2-} + 2e^-$, $Zn(OH)_4^{2-} \rightarrow ZnO +$

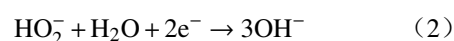
$H_2O + 2OH^-$; 空气阴极, $O_2 + 4e^- + 2H_2O \rightleftharpoons 4OH^-$; 总反应, $2Zn + O_2 \rightarrow 2ZnO$.

ZABs 在放电和充电时, 空气电极分别发生 ORR 和 OER 反应, 然而, ORR 和 OER 涉及四电子和四质子的转移, 动力学缓慢, 往往需要较高的过电势, 这制约了 ZABs 的充放电性能^[13], 因此, 高活性、高稳定性的 ORR/OER 双功能催化剂是 ZABs 的关键材料. 目前已经被广泛研究的 ORR/OER 双功能催化剂主要可以分为两大类贵金属催化剂和非贵金属催化剂, 其中, 贵金属催化剂主要包括用于 OER 的 Ir 和 Ru 基催化剂和用于 ORR 的 Pt 催化剂. 非贵金属又可以具体分为无金属材料(如杂原子掺杂碳, 富含缺陷的纳米碳材料), 基于 MOF 的催化剂(包括原始 MOF 及其衍生物), 各类非贵金属基材料(如过渡金属及其合金, 过渡金属氧化物, 过渡金属基复合材料, 过渡金属单原子材料等)^[14-18].

本文综述了不同种类的过渡金属氧化物 ORR/OER 双功能催化剂, 介绍了各类催化剂的活性来源及其在 ZABs 能量密度、充/放电电压、稳定性等方面的表现, 总结了当下研究现状中提高其催化性能的方法.

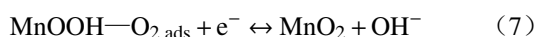
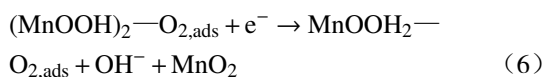
1 锰氧化物

在所有单一过渡金属氧化物基 ORR/OER 双功能催化剂中, 锰氧化物(MnO_x)是最常见的候选材料, 具有成本低、储量丰富、环境友好的优点^[19]. Mao 等^[20]认为 MnO_x 的 ORR 催化机制可以通过以下几个步骤来描述:



ORR 遵循四电子机制, O₂ 经过反应(1)生成

HO_2^- , 然后发生得电子还原反应(2)或者歧化反应(3)生成 OH^- , 其中, MnO_x 对反应(3)具有高催化活性从而加快了整体 ORR 反应速度. Roche 等^[21]认为 MnO_x 中存在大量 $\text{Mn}^{\text{III}}/\text{Mn}^{\text{IV}}$ 氧化还原电子对, 可作为氧受体-供体, 具体而言, 首先 MnO_2 中插入质子形成 MnOOH (反应(4)), 随后氧分子吸附到两个相邻的 MnOOH 位点(桥接吸附位点)上(反应(5)), MnOOH 与氧气分子结合生成 OH^- (反应(6)), 而反应(7)是 O_{ads} (吸附氧)物种的还原, 该四电子反应途径可使 O_2 还原为 OH^- . 同样地, OER 作为 ORR 的逆反应, 也有研究表明 MnO_x 催化剂的 OER 活性与锰的可变价态相关^[22-23].



为了研究不同晶体结构对锰氧化物催化性能的影响, Meng 等^[24]制备了 α 相、 β 相、 δ 相和无定形等不同相的 MnO_2 材料, 对比了这些材料在碱性介质中的电催化性能. 结果表明, 在 ORR 或者 OER 中 MnO_2 的电催化活性都强烈依赖于晶体结构, 并且遵循 $\alpha\text{-MnO}_2$ 电催化活性 > 无定形 MnO_2 电催化活性 > $\beta\text{-MnO}_2$ 电催化活性 > $\delta\text{-MnO}_2$ 电催化活性这一趋势. 其中 $\alpha\text{-MnO}_2$ 的高电催化活性可归因于以下两点: 一是 $\alpha\text{-MnO}_2$ 中由角与边缘共享的 MnO_6 八面体可组成 2×2 隧道结构, 相比于 $\beta\text{-MnO}_2$ 的 1×1 隧道结构、 $\delta\text{-MnO}_2$ 的 1×2 和 1×1 隧道结构, 可容纳更多的氧气分子、阳离子与水分子(如图 1 所示), 从而提供了更多的活性位点; 二是 $\alpha\text{-MnO}_2$ 具有混合价态($\text{Mn}^{3+}/\text{Mn}^{4+}$), 可通过 Mn^{3+} 和 Mn^{4+} 之间的氧化还原来促进 OER 过程中的电荷转移.

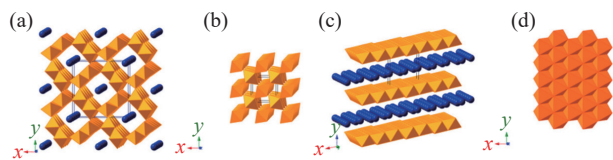


图 1 晶体结构^[24]. (a) $\alpha\text{-MnO}_2$ (2×2 隧道); (b) $\beta\text{-MnO}_2$ (1×1 隧道); (c) $\delta\text{-MnO}_2$ (层状); (d) 无定形氧化锰

Fig.1 Crystalline structures^[24]: (a) $\alpha\text{-MnO}_2$ (2×2 tunnel); (b) $\beta\text{-MnO}_2$ (1×1 tunnel); (c) $\delta\text{-MnO}_2$ (layered); (d) amorphous manganese oxide

作为改变纳米材料电子结构的有效手段之一, 金属原子掺杂也可用于提高 MnO_x 基催化剂的活性. 已有文献报道使用 Co^{2+} 、 Ag^+ 、 Fe^{3+} 、 Ni^{2+} 、

Mo^{6+} 、 Cu^{2+} 、 Cr^{3+} 、 V^{5+} 等不同金属离子对 MnO_2 进行掺杂^[25-27]. $\alpha\text{-MnO}_2$ 的 (2×2) 隧道结构是由内部存在的水分子和阳离子支撑, 而该隧道结构的坍塌会引发相变, 转化为 $\beta\text{-MnO}_2$ ^[28]. 在低价态阳离子掺杂的 MnO_x 中, 晶格的负电荷多, 可以促使溶液中更多的 K^+ 等阳离子进入到隧道中, 从而提高 $\alpha\text{-MnO}_2$ 结构稳定性. 而掺杂高价态阳离子会产生过量正电荷, 阻碍阳离子进入隧道结构, 影响 $\alpha\text{-MnO}_2$ 稳定性, 降低催化活性. 此外, MnO_2 常常表现出较差的导电性, 杂原子掺杂还可加快电子传输速率, 从而提高 ZABs 的放/充电速率^[29-31]. Bôas 等^[32]制备了 Bi^{3+} 和 Ce^{4+} 掺杂的 MnO_2 纳米棒, 用作碱性介质中 ORR 和 OER 电催化时, 两种催化剂的电荷转移电阻都比未掺杂样品低得多, 其 ORR 半波电位与 $10 \text{ mA} \cdot \text{cm}^{-2}$ 电流密度下的 OER 电位 (E_{10}) 的差值 ΔE 分别为 1.07 V 和 1.02 V. 其中, Ce^{4+} 掺杂 MnO_2 纳米棒 ZABs 的峰值功率密度为 $45 \text{ mW} \cdot \text{cm}^{-2}$, 高于 MnO_2 材料 ZABs 的 $40 \text{ mW} \cdot \text{cm}^{-2}$, 表明其良好的阴极催化作用.

除了对 MnO_x 进行金属元素掺杂外, 将其与碳、碳化物等电导率高的材料复合, 也是克服其低电导的有效策略. Song 等^[33]通过水热合成法在 TiC 纳米颗粒上沉积非晶态 MnO_x , 该材料作为 ZABs 氧电极, 具有高效、抗腐蚀的优点, 表现出与 Pt/C 相当的 ORR 起始电位 (0.96 V) 和半波电位 ($E_{1/2}$, 0.8 V), 比 IrO_2 更低的 OER 过电位 (1.56 V), 更低的 Tafel 斜率 (ORR, $72 \text{ mV} \cdot \text{dec}^{-1}$; OER, $110 \text{ mV} \cdot \text{dec}^{-1}$). Pandey 等^[34]以次氨基三乙酸 (NTA) 和乙酸锰为前体, 采用水热法合成了一种 MnO_x 和氮掺杂碳复合的双功能氧催化剂(如图 2 所示), 其中, 氮掺杂碳形成 (NC) 的多孔网络显著提高电催化中的电导和传质, MnO_x 中 Mn 阳离子的混合氧化态以及碳基体中高比例的氮掺杂也有利于 ORR 和 OER 催化.

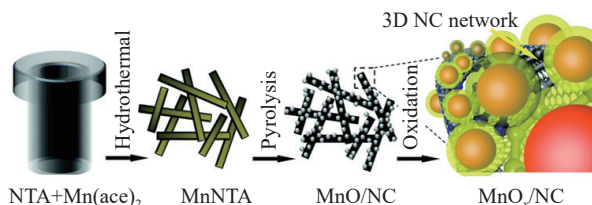


图 2 分级多孔 MnO_x /氮掺杂碳(MnO_x/NC)纳米棒催化剂的合成流程示意图^[35]

Fig.2 Schematic of the synthesis procedure of the hierarchically porous MnO_x/NC nanorod catalyst^[35]

Chen 等^[35]通过化学浴沉积方法在碳布上原位生长 MnO_x 纳米片, 所得材料表现出良好的 ORR

和 OER 双功能活性, ORR 催化活性与 Pt/C 相当, 并且在 $10 \text{ mA} \cdot \text{cm}^{-2}$ 的电流密度下 OER 过电位仅为 388 mV . 组装而成的柔性全固态 ZABs 表现优异, 放电电压高达 1.3 V , 充电电压仅为 1.9 V , 可稳定运行 45 h , 120 次循环后的往返能量效率为 62.4% . Lu 等^[19] 以双金属-有机骨架材料为前驱体, 通过水热与煅烧合成了一种 $\text{MnO}/\text{Co}/$ 多孔石墨碳复合材料, 其中, 原位生成的 Co 纳米晶促进了碳的石墨化, 提高了高电导率, 异质界面也提高了 OER 活性. Ji 等^[36] 以羧基修饰的碳纳米管作为核心前体来稳定不同金属离子, 采用静电纺丝-煅烧工艺, 在多孔碳纳米纤维中实现了丰富的 $\text{Ni}|\text{MnO}$ 异质界面(如图 3 所示), 得益于一维纤维组成的三维多孔网络结构和异种金属位点之间的强界面作用, 催化剂表现出低至 0.763 V 的 ΔE 值, 由其组装而成的 ZABs 具有高的开路电压、功率密度和长循环寿命. 表 1 列举出了最近报导的一些锰氧化物 ORR/OER 双功能催化剂的具体性能.

2 尖晶石型

尖晶石是一类化学式为 AB_2O_4 的过渡金属

氧化物, 其中氧离子呈立方紧密堆积, A 阳离子可以处于 +2 或 +4 氧化态, B 阳离子可以处于 +3 或 +2 氧化态, 可表示为 $\text{A}^{2+}\text{B}_2^{3+}\text{O}_4^{2-}$ 和 $\text{A}^{4+}\text{B}_2^{2+}\text{O}_4^{2-}$ (图 4(a))^[44].

尖晶石型材料中有两种金属位点, 四面体位点和八面体位点. 活性位点对氧中间体(例如 OH^* 、 O^* 、 OOH^*)吸附能被认为决定了 ORR/OER 反应中的能垒和限速步骤. 对于尖晶石氧化物来说, 氧中间体吸附于配位不饱和的表面金属位点上, 由于八面体配位的金属离子与氧之间的相互作用更强, 其被认为是氧电催化的活性位点. 具体而言, 对于八面体配位的金属离子, d 轨道分裂为低能级的 t_{2g} 轨道和高能级的 e_g 轨道, 当与 O 成键时, e_g 轨道直接指向 O, 与 O_{2p} 轨道产生大的空间重叠, 导致强的化学相互作用. Wei 等^[45] 通过调整合成条件和金属离子的类型来调节尖晶石催化剂八面体位点金属离子的 e_g 轨道占有率, 结果表明, ORR 和 OER 活性与尖晶石八面体位点 e_g 轨道占用率对应的火山图如图 4(b)、(c) 所示, 证实尖晶石材料中的八面体金属离子是氧电催化的活性位点, 其 e_g 轨道的占有率决定尖晶石型材料的催化活性^[46-47].

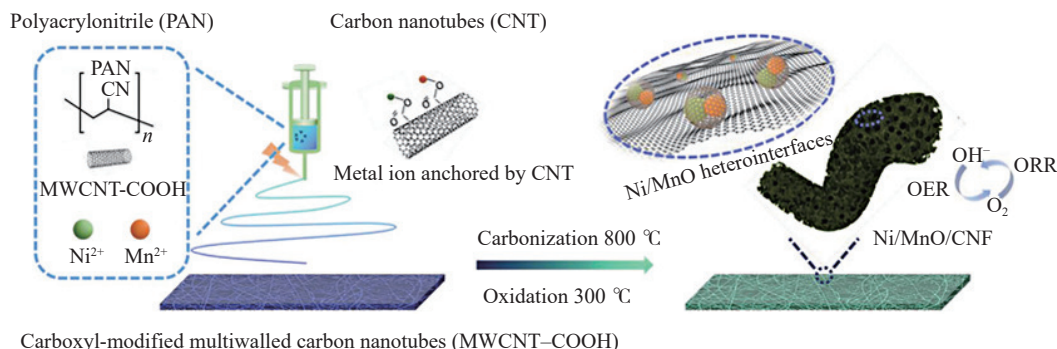


图 3 Ni|MnO 制备流程图^[36]

Fig.3 Fabrication process^[36]

表 1 一些锰氧化物 ORR/OER 双功能催化剂的具体性能

Table 1 Properties of some recently reported manganese oxide ORR/OER bifunctional catalysts

Reference	Electrocatalyst	Loading/ ($\text{mg} \cdot \text{cm}^{-2}$)	$\Delta E/\text{V}$	$E_{1/2}/\text{V}(\text{vs RHE})$	$E_{10}/\text{V}(\text{vs RHE})$	Electrolyte
[37]	$\text{MnO}@/\text{Co}-\text{N}/\text{C}$	0.6	0.93	0.83	1.76	$0.1 \text{ mol} \cdot \text{L}^{-1} \text{ KOH}$
[38]	$\text{MnVO}_x@/\text{N}-\text{rGO}$	0.3	0.85	0.8	1.65	$0.1 \text{ mol} \cdot \text{L}^{-1} \text{ KOH}$
[39]	MnO_2 (KIT-6)	0.204	1.28	0.56	1.84	$0.1 \text{ mol} \cdot \text{L}^{-1} \text{ KOH}$
[36]	$\text{Ni} \text{MnO}/\text{CNF}$	0.2	0.763	0.826	1.589	$0.1 \text{ mol} \cdot \text{L}^{-1} \text{ KOH}$
[40]	$\text{NiO}/\text{MnO}_2@/\text{PANI}$	0.245	0.74	0.83	1.57	$0.1 \text{ mol} \cdot \text{L}^{-1} \text{ KOH}$
[41]	MnO_2-NiFe		0.65	0.8	1.45	$0.1 \text{ mol} \cdot \text{L}^{-1} \text{ KOH}$
[42]	$\text{NiFeO}@/\text{MnO}_x$	0.1	0.825	0.805	1.63	$0.1 \text{ mol} \cdot \text{L}^{-1} \text{ KOH}$
[43]	$\text{np-RuO}_2/\text{nr-MnO}_2$	0.3	0.69	0.61	1.3	$0.1 \text{ mol} \cdot \text{L}^{-1} \text{ KOH}$
[33]	$\text{a-MnO}_x/\text{TiC NPs}$	0.44	0.76	0.8	1.56	$0.1 \text{ mol} \cdot \text{L}^{-1} \text{ KOH}$

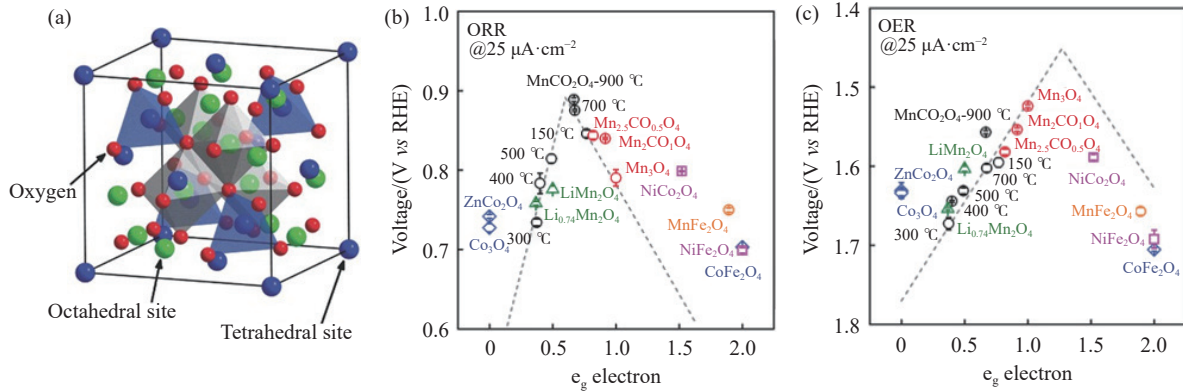
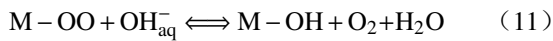
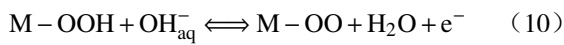
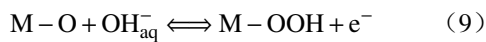
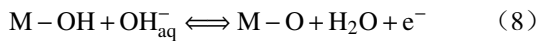


图 4 尖晶石的 (a) 晶体结构示意图^[44], (b) ORR 火山图和 (c) OER 火山图^[48]

Fig.4 (a) Crystal structure^[44], (b) ORR and (c) OER volcano plots^[48]

对于四面体配位的金属离子来说, 其 t_{2g} 轨道和 e_g 轨道指向明显偏离四个相邻氧的方向, 产生轨道重叠较少. 尖晶石中, 每个氧阴离子由一个四面体阳离子和三个八面体阳离子共享, 四面体的组成会影响氧阴离子和占据八面体的阳离子之间的键合行为, 当具有不同电负性的阳离子占据四面体位点时, 八面体配位的金属离子以及氧阴离子上的电荷分布也会发生变化, 从而对其催化活性产生影响. 对于碱性条件下的 ORR/OER 反应来说, 尖晶石的催化过程可以被视为沿着如图 5(b) 和 (c) 所示的反应环进行, 包括氧的吸附和解吸、电子和质子的转移这四个步骤, 同时伴有多个价态的活性过渡金属阳离子的可逆氧化还原反应^[48]. 其反应过程如下所示



具体来说, 对于 OER 而言, 其反应过程可分为以下四个步骤: (1) 失去电子并形成吸附原子 O 和 H_2O ; (2) OH^- 阴离子与吸附的 O 原子反应生成吸附的 OOH 物种; (3) 吸附的 OOH 物种进一步与额外的 OH^- 阴离子反应形成 H_2O 和吸附的 O_2 ; (4) 吸附的 O_2 从催化剂表面脱离. 对于 ORR 而言, 其反应步骤如下: (1) OO^{2-}/OH^- 置换; (2) 表面过氧化物物质的形成; (3) 表面氧化物的形成; (4) 表面氢氧化物物质的再生^[49-51].

合理改变尖晶石氧化物的组分可实现催化剂 ORR/OER 活性的调控, 二元尖晶石氧化物如 $Ni_xCo_{3-x}O_4$ 、 $Mn_xCo_{3-x}O_4$ 、 $Zn_xCo_{3-x}O_4$ 和 $Cu_xCo_{3-x}O_4$ 等的催化性能已经被广泛研究^[52-56]. Liu 等^[57] 采用水热法合成 $ZnCo_2O_4$ /氮掺杂碳纳米管 ($ZnCo_2O_4/N-CNT$) 复合催化剂, 其在 $10 mA \cdot cm^{-2}$ 电流密度下 OER 过电位为 1.65 V, 低于 $Co_3O_4/N-CNT$ 的 1.67 V 和 $ZnCo_2O_4$ 的 1.69 V, 具有更低的 Tafel 斜率, 并且其 ORR 起始电位 (0.95 V) 和半波电位 (0.87 V) 都接近商业 Pt/C 催化剂, 优于 $Co_3O_4/N-CNT$. Jiang^[58] 等通过引入 Zn 来调整氮掺杂碳纳米管 (氮掺杂碳纳

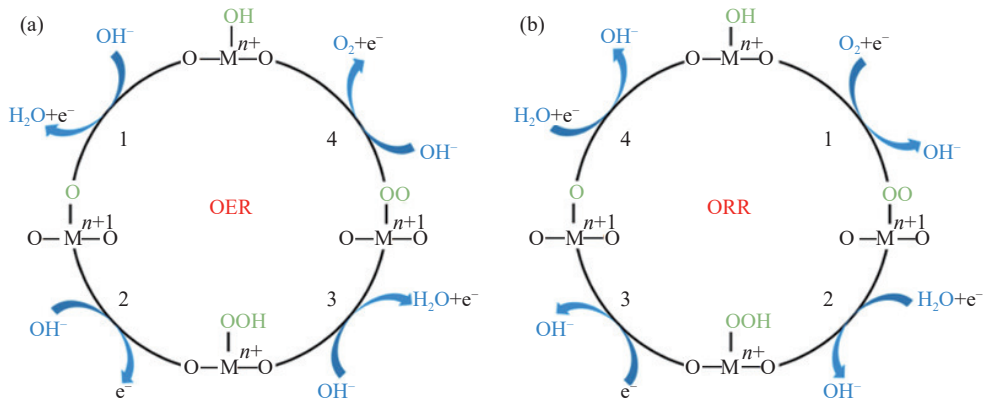


图 5 碱性条件下的尖晶石氧化物 (a) OER 反应环, (b) ORR 反应环^[47]

Fig.5 Spinel oxides under alkaline conditions (a) OER reaction ring, (b) ORR reaction ring^[47]

米管: NCNTs, 碳纳米管: CNTs) 锚定的立方尖晶石结构 ($Zn_xNi_{1-x}Co_2O_4$), 发现 $Zn_{0.4}Ni_{0.6}Co_2O_4$ 材料的 OER 和 ORR 活性较高. Rao 等^[59] 通过对 Co_3O_4 进行 V 掺杂, 使 e_g 占有率优化到理想的 1.0, 有效地平衡了氧中间体在 ORR 和 OER 速率决定步骤中的吸附能, 作为 ORR/OER 双功能电催化剂, 其性能优于 Pt-

IrO_2 的组合. Wang 等^[60] 合成了一系列氮掺杂碳纳米管负载的钴基尖晶石氧化物电催化剂 (如图 6 所示) (CNTs: 碳纳米管), 其中 $MnCo_2O_4$ 对 ORR/OER 反应表现出最高的活性和耐久性, 装配的 ZABs 可提供 $827\text{ mA}\cdot\text{h}\cdot\text{g}^{-1}(\text{Zn})$ 的比容量和 $74.63\text{ mW}\cdot\text{cm}^{-2}$ 的功率密度, 并且在 300 次循环后电压没有下降.

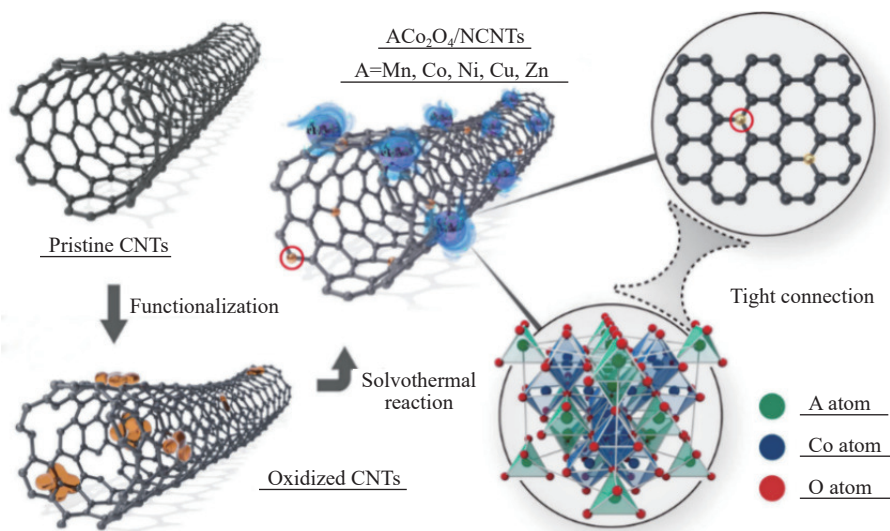


图 6 ACo_2O_4 ($A=Mn, Co, Ni, Cu, Zn$) 氮掺杂碳纳米管 (NCNTs) 催化剂的制备过程示意图^[60]

Fig.6 Schematic of the formation process of $ACo_2O_4/NCNTs$ ($A = Mn, Co, Ni, Cu, \text{ and } Zn$)^[60]

此外, 大多数尖晶石氧化物都存在导电性差和结构坚固性低的问题, 有些还具有较差的 O_2 结合和活化能力. 因此, 将尖晶石氧化物与碳载体 (如石墨烯、碳纳米管、碳纳米纤维和炭黑等) 或其他金属进行复合, 来提高材料的 ORR 催化性能, 并且形成导电网络促进电荷转移, 也是常用的策略之一^[61-64]. 尖晶石与碳载体的复合还能增强其分散均匀性, 防止颗粒团聚, 并提供额外的表面积. Jiang 等^[65] 合成出负载了 Co_3O_4 的氮和硼元素共掺杂石墨烯空心球, 该材料表现出比商业 $Pt/C+RuO_2/C$ 更高的 ORR/OER 电催化活性和耐久性. Li 等^[66] 合成了一种氮掺杂碳骨架负载 Co_3O_4 纳米晶的石榴状电催化剂 (如图 7(a), (b), (c), (d) 所示), 该催化剂中, 小尺寸 Co_3O_4 纳米颗粒提供了丰富的活性位点, 而石榴状结构碳基体能够有效防止金属氧化物团聚并提供传质通道, 从而增强了催化活性和耐用性. Chen 等^[67] 采用静电纺丝技术将细小均匀的尖晶石钴锰氧化物纳米颗粒嵌入到氮掺杂碳纳米纤维中, 形成复合催化剂. 其中, 纳米纤维组成的三维导电网络同样起到了加快物质扩散、电荷转移和暴露活性位点的作用, 也抑制了氧化物纳米粒子的团聚和脱离. Jiang 等^[58] 通过 Co^{2+} 离子与

Zn 有机骨架纳米片之间进行离子交换和还原反应, 合成了一种多孔碳壳负载 Co/Co_3O_4 复合纳米粒子 ($Co/Co_3O_4@PGS$) (如图 7(e) 所示), 该电催化剂 ORR 半波电位比 Pt/C 高 15 mV, 在 $10\text{ mA}\cdot\text{cm}^{-2}$ 时的 OER 过电位比 Ir/C 低 60 mV, 当集成在 ZABs 中时, 其在 $10\text{ mA}\cdot\text{cm}^{-2}$ 下稳定循环超过 800 h. 表 2 总结了一些最近报导的尖晶石型 ORR/OER 双功能电催化剂的性能.

3 钙钛矿型

钙钛矿是一类化学式为 ABO_3 的过渡金属氧化物, 其中 A 为稀土金属或碱土金属, B 为过渡金属, 其中较大尺寸的稀土或碱金属阳离子占据与 12 个 O 进行配位的 A 位点, 较小尺寸的过渡金属阳离子占据与 6 个 O 配位的 B 位点, 呈立方结构 (如图 8(a) 所示)^[91]. 对于钙钛矿氧化物, 一般认为占据 B 位点的金属原子为其 ORR 活性位点, ORR 催化被认为沿着图 8(b) 所示的路径进行^[92]. 氧空位可以增加 ORR 电子转移数以减少过氧化物的形成, 此外, 氧空位的存在使晶格氧在钙钛矿表面移动, 降低了氧迁移的屏障, 使氧更容易迁移到电极材料内部^[93].

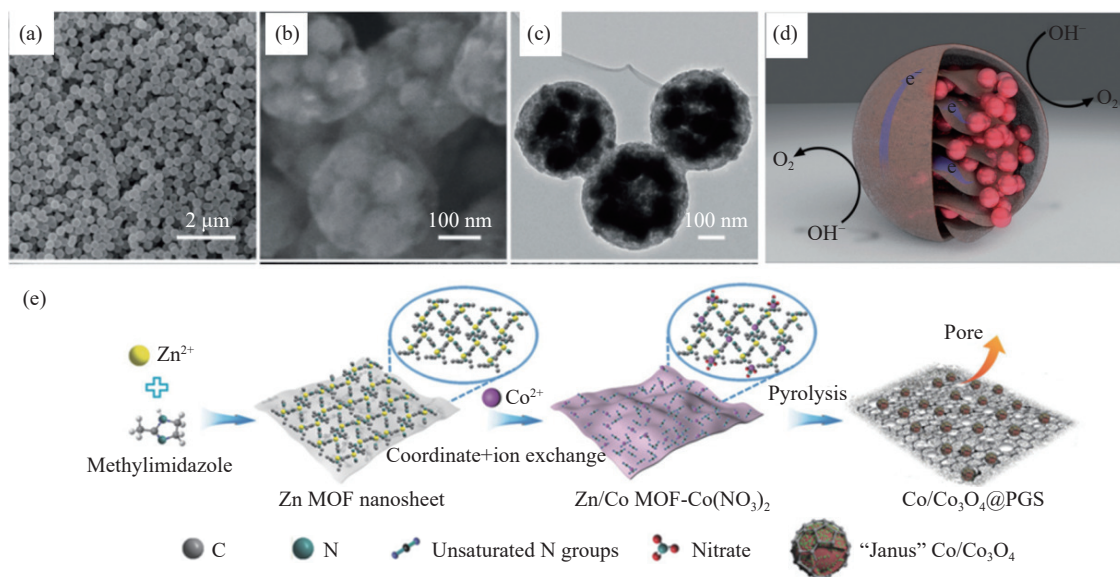


图 7 氮掺杂碳骨架负载 Co_3O_4 纳米晶的石榴状电催化剂的(a, b)SEM 图像, (c)TEM 图像和(d)示意图^[66]; (e) $\text{Co}/\text{Co}_3\text{O}_4@PGS$ 制备示意图^[58]

Fig.7 (a, b) SEM images, (c) TEM images, and (d) illustration of the electrocatalyst of the Co_3O_4 nanocrystals embedded in a nitrogen-doped partially graphitized carbon framework with a unique pomegranate-like composite architecture^[66]; (e) illustration of the synthesis process for preparing interpenetrating Co and Co_3O_4 nanoparticles stitched in porous graphitized shells ($\text{Co}/\text{Co}_3\text{O}_4@PGS$)^[58]

对于钙钛矿氧化物的 OER 机制, 有表面吸附 (Adsorbate evolution mechanism, AEM) (Me_1) 和晶格氧交换 (Lattice oxygen oxidation mechanism, LOM) (Me_2) 两种机制^[94]. 如图 9(a) 所示, AEM 的第一步是羟基(OH)吸附过程(Me_1 -1 步)(后缀“-1”代表反应过程的第一步, 依此类推), 羟基与 B 位金属位点以形成相对稳定的状态($\text{M}-\text{OH}$), 接着, 吸附物发生脱氢反应, 生成表面吸附氧 MO(Me_1 -2 步)^[95]. 吸附氧继续与 OH 反应形成 $\text{M}-\text{OOH}$ (Me_1 -3 步), 最后, 吸附物使第二个 H 脱氢并形成 $\text{MO}=\text{O}$, 然后释放出氧(Me_1 -4 步). 由于大多数钙钛矿在 Me_1 -2 步中具有相对较高的能垒, Me_1 -2 步通常是其 OER 的速率决定步骤. 而对 LOM 机制来说(图 9(b)), 第一步始于晶格中的氧空位(Me_2 -1 步), 第二步中, 催化剂的相邻位点吸附了一个额外的羟基 $\text{M}_1-\text{OH}/\text{M}_2-\text{OH}$, 称为羟基填充步骤(Me_2 -2 步), 此步骤比 AEM 中吸附氧的形成具有更低的能垒. 羟基脱氢困难形成过渡态, 过渡态不稳定, 最终变为 $\text{M}_1-\text{O}=\text{O}/\text{M}_2$ (Me_2 -3 步), 最后释放氧, 通过填充羟基恢复初始状态 $\text{M}_1-\text{OH}/\text{M}_2$ (Me_2 -4 步). 虽然 LOM 似乎打破了 Me_1 -2 带来的更高能垒, 但据报道只有少数高共价钙钛矿发生 LOM. 除了 AEM 和 LOM, 一些催化剂还表现出 O—O 耦合机制(Me_3)(图 9(c)), 这些催化剂对 Me_1 -2 步骤没有高能垒, 但它们的 Me_1 -3 能垒较高. 在这种情况下, 催化剂表面形成了大量的 MO, 且很难进一步形成 $\text{M}-\text{OOH}$. 当 MO 难以转化为 $\text{M}-\text{OOH}$ 时, 两个 MO 会直接相互偶

联(Me_3 -2), 生成一个氧分子(Me_3 -3). 然而, 这种机制通常很难实现, 需要两个相邻的吸附氧和高能垒^[96].

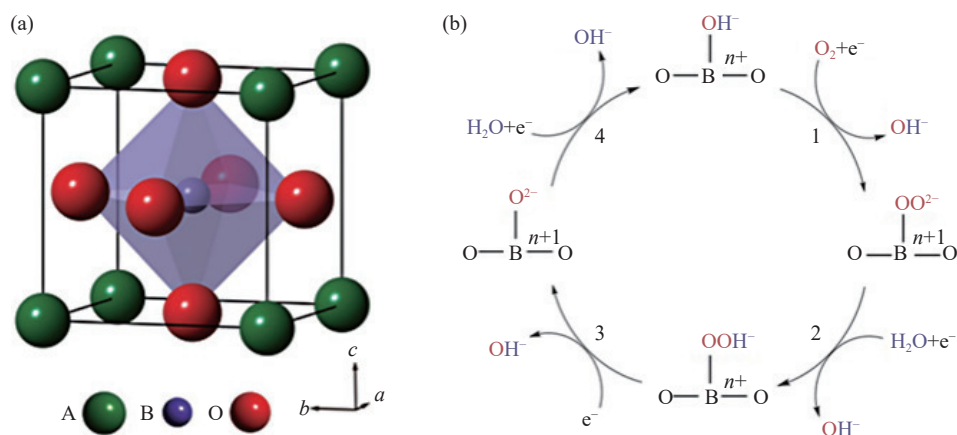
与尖晶石相似, 钙钛矿氧化物的 B 位过渡金属的电子结构也对其催化性能有着重大的影响. Suntivich 等^[97] 使用分子轨道理论证明, 钙钛矿型催化剂的 ORR 活性与 B 位阳离子 e_g 轨道的占据率呈火山型关系. 从图 10(a) 可以清楚地看出, 在 e_g 轨道占据率约为 1 的钙钛矿, 如 LaMnO_3 、 LaCoO_3 和 LaNiO_3 , 表现出最高的 ORR 活性. e_g 轨道填充过少的 $\text{La}_{1-x}\text{Ca}_x\text{CrO}_3$ (e_g 占据数 ≈ 0) 和 e_g 轨道填充过多的 $\text{La}_{1-x}\text{Ca}_x\text{FeO}_3$ (e_g 占据数 ≈ 2) 显示出较低的 ORR 活性. 以 e_g 轨道占据率作为描述符 ORR 活性遵循 Sabatier 原理, 即 e_g 轨道占用过少或占用过多会导致与含氧中间体的吸附太强或太弱, 从而影响其催化活性. 在另一项研究中, 他们运用相同的描述符来预测钙钛矿的 OER 活性, 如图 10(b) 所示^[98], 对于所测试的钙钛矿, 观察到了类似的火山型相关性, $\text{Ba}_{0.5}\text{Sr}_{0.5}\text{Co}_{0.8}\text{Fe}_{0.2}\text{O}_{3-\delta}$ 钙钛矿 e_g 轨道占据数为 1.2, 显示出最高的 OER 活性.

相比于其他过渡金属氧化物, 钙钛矿氧化物由于其 A 位和 B 位均可由其他碱土、稀土金属或者过渡金属部分取代, 因此钙钛矿氧化物种类更为丰富, 更易调控其电子结构和催化性能. 最近报道的一些钙钛矿在碱性条件下的 ORR/OER 性能已经达到甚至超过了基于贵金属(即 Pt、Ir 和 Ru)的催化剂的性能. 传统的固态反应合成钙钛矿氧

表 2 一些最近报道的尖晶石型电催化剂的双功能性能

Table 2 ORR/OER bifunctional performances of some recently reported spinel-based electrocatalysts

Reference	Electrocatalyst	Loading/(mg·cm ⁻²)	$\Delta E/V$	$E_{1/2}/V(\text{vs RHE})$	$E_{10}/V(\text{vs RHE})$	Electrolyte
[68]	CMO		0.95	0.74	1.69	0.1 mol·L ⁻¹ KOH
[69]	NiCo ₂ S ₄ HSs	0.5	0.83	0.8	1.63	0.1 mol·L ⁻¹ KOH
[70]	CoFe ₂ O ₄	0.15	0.91	0.73	1.64	0.1 mol·L ⁻¹ KOH
[70]	MnFe ₂ O ₄	0.15	1.11	0.71	1.82	0.1 mol·L ⁻¹ KOH
[70]	NiFe ₂ O ₄	0.15	0.96	0.68	1.64	0.1 mol·L ⁻¹ KOH
[65]	Co ₃ O ₄ /NBGHSSs	0.13	0.838	0.862	1.7	0.1 mol·L ⁻¹ KOH
[66]	Co ₃ O ₄ /NPGC	0.2	0.838	0.842	1.68	0.1 mol·L ⁻¹ KOH
[71]	Ni/NiO/NiCo ₂ O ₄ /N-CNT	0.24	0.87	0.74	1.51	0.1 mol·L ⁻¹ KOH
[72]	Co ₃ O ₄ /NHPC	0.38	0.815	0.835	1.65	0.1 mol·L ⁻¹ KOH
[73]	NiCoO ₂ /CNTs	0.51	0.99	0.67	1.66	0.1 mol·L ⁻¹ KOH
[74]	NiCoMnO ₄ /N-rGO	0.225	0.99	0.75	1.74	0.1 mol·L ⁻¹ KOH
[75]	Co ₃ O ₄ /N-rmGO	0.24	0.8	0.8	1.6	0.1 mol·L ⁻¹ KOH
[76]	NiCo ₂ S ₄ @N/S-rGO	0.283	~ 0.93	~ 0.79	~ 1.72	0.1 mol·L ⁻¹ KOH
[77]	NiCo ₂ S ₄ /N-CNT	0.248	0.8	0.8	1.6	0.1 mol·L ⁻¹ KOH
[63]	NiCo ₂ O ₄ /Co ₃ N-CNTs	0.5	0.707	0.862	1.569	0.1 mol·L ⁻¹ KOH
[78]	NCYS	0.64	0.93	0.81	1.74	0.1 mol·L ⁻¹ KOH
[79]	MnCo ₂ O _{4.5}	0.275	1	0.7	1.7	0.1 mol·L ⁻¹ KOH
[80]	NCO-10	0.2	0.9	0.73	1.63	0.1 mol·L ⁻¹ KOH
[81]	LT-Li _{0.5} CoO ₂	0.25	0.93	0.64	1.57	0.1 mol·L ⁻¹ KOH
[82]	CuCo ₂ S ₄ NSs	0.2	0.817	0.7	1.517	0.1 mol·L ⁻¹ KOH
[83]	MnFe ₂ O ₄		1.05	0.72	1.77	0.1 mol·L ⁻¹ KOH
[84]	5%Ni-Co	0.408	0.78	0.83	1.61	0.1 mol·L ⁻¹ KOH
[55]	MnFe ₂ O ₄ /NiCo ₂ O ₄	0.3	0.807	0.767	1.574	0.1 mol·L ⁻¹ KOH
[85]	PdCo-300	0.455	0.75	0.83	1.58	0.1 mol·L ⁻¹ KOH
[86]	Pd@PdO-Co ₃ O ₄		0.813	0.727	1.54	0.1 mol·L ⁻¹ KOH
[87]	GM-Co-B-N	0.16	0.8	0.8	1.6	0.1 mol·L ⁻¹ KOH
[88]	CCO@C	0.1	0.69	0.87	1.56	0.1 mol·L ⁻¹ KOH
[89]	NiCo ₂ S ₄ /RGO	0.28 ⁿ	0.91	0.78	1.69	0.1 mol·L ⁻¹ KOH
[90]	Co ₃ O ₄ @POF	0.24	0.74	0.82	1.56	0.1 mol·L ⁻¹ KOH

图 8 (a) 钙钛矿氧化物理想晶胞的示意图^[91], (b) 钙钛矿氧化物的 ORR 催化反应途径^[92]Fig.8 (a) Schematic of the ideal unit cell^[91] and (b) proposed oxygen reduction reaction pathway of perovskite oxide^[92]

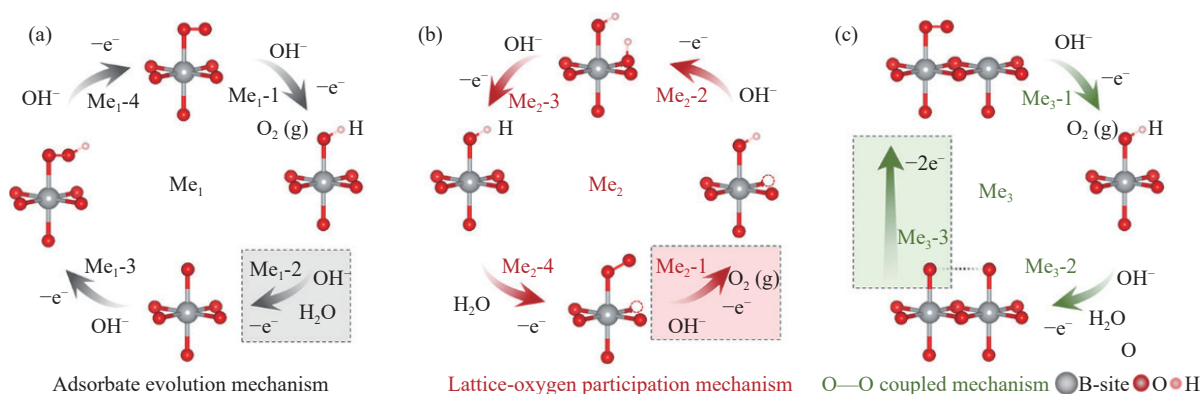


图9 钙钛矿八面体 B 位金属位点的不同 OER 机制(红色和灰色原子分别代表氧和 B 位阳离子,虚线框表示速率确定步骤^[95]。(a) AEM 机制;(b) LOM 机制;(c) O—O 耦合机制。

Fig.9 Different OER mechanisms of the octahedral B site in perovskite (the red and gray atoms donate oxygen and B site, respectively. The dotted box represents the rate-determining step)^[95]: (a) AEM; (b) LOM; (c) O—O coupled mechanism

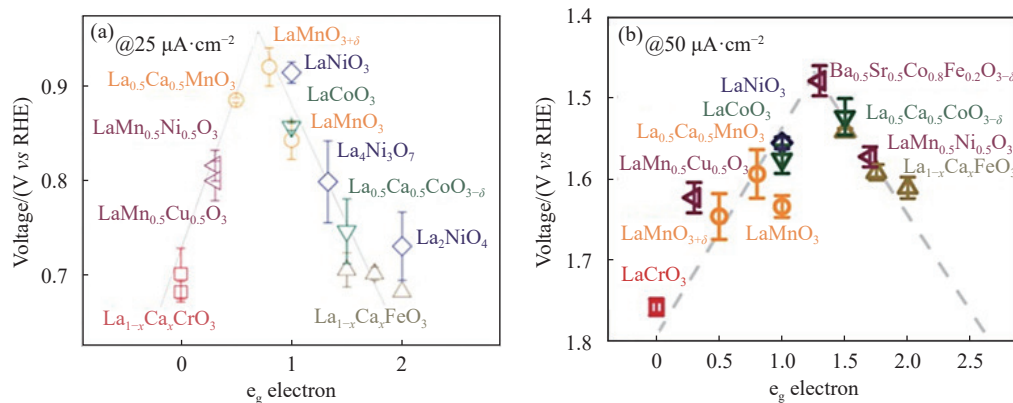


图10 (a)某些钙钛矿氧化物中 ORR 电流为 $25 \mu\text{A}\cdot\text{cm}^{-2}$ 的电位与 e_g 轨道的函数关系;(b)某些钙钛矿基氧化物中 OER 电流 $50\mu\text{A}\cdot\text{cm}^{-2}$ 处的电位与 e_g 轨道的关系^[98]。

Fig.10 (a) Potentials at $25 \mu\text{A}\cdot\text{cm}^{-2}$ of the ORR current as a function of the e_g orbital in some perovskite-based oxides; (b) potentials at $50 \mu\text{A}\cdot\text{cm}^{-2}$ of the OER current as a function of the e_g orbital in some perovskite-based oxides^[98]

化物往往需要长时间的高温来克服扩散障碍、形成钙钛矿晶体结构。这种方法的主要问题是钙钛矿相的纯度不够,且由于高温团聚而造成比表面积减小。通过结合一些新的工艺,比如溶胶-凝胶法、共沉淀水解、反胶束合成、水热法等,可以部分改善上述问题^[99-103]。Cai 等^[104]设计了一种固态凝胶工艺制备 $\text{LaMnO}_{3+\delta}$ 钙钛矿氧化物气凝胶,将其 $\text{LaMnO}_{3+\delta}$ 纳米颗粒沉积到多孔碳基质颗粒上,在高温下快速加热,碳被燃烧,形成互连的三维钙钛矿气凝胶结构体。该材料密度低、孔隙率高、比表面积大,促进了碱性介质中的 ORR 反应动力学,在 0.8 V 电位下,质量活度为 $66.2 \text{ A}\cdot\text{g}^{-1}$,是传统块状 LaMnO_3 的 153 倍。Kuai 等^[105]通过硝酸盐溶液喷雾热解法制备了一种介孔 $\text{LaMnO}_{3+\delta}$ 空心微球,其工艺流程为,将含有 $\text{Mn}(\text{NO}_3)_2$ 、 $\text{La}(\text{NO}_3)_3$ 和嵌段共聚物的溶液通过超声波加湿器雾化,吸入管式炉后,在空气中 700°C 煅烧 4 h 后得到 $\text{LaMnO}_{3+\delta}$

微球,用此方法所制备的钙钛矿微球有着尺寸小、多孔、比表面积大等优点(如图 11 所示)。

提高钙钛矿催化活性的一种方法是调整 A 位碱金属或稀土金属或 B 位过渡金属阳离子种类。杂原子掺杂会造成钙钛矿中的原子和电荷重排以及价态变化,从而影响其催化活性。对于钙钛矿氧化物的 A 位掺杂, Aziz^[106]等研究了不同含量的 La 掺杂对钙钛矿 $\text{Sr}_{2-x}\text{La}_x\text{FeO}_6$ ($x=0.25, 0.5$ 和 1) 的影响,发现其晶粒形态、电阻率和电化学活性都受到 La 掺杂的强烈影响,其中 $\text{Sr}_{1.5}\text{La}_{0.5}\text{FeO}_6$ 在 $0.1 \text{ mol}\cdot\text{L}^{-1}$ KOH 碱性溶液中表现出最优异的 ORR 和 OER 电化学活性。不同 A 位碱金属的掺杂会改变钙钛矿的八面体堆叠构型,从而对钙钛矿催化活性造成影响。Zhao 等^[107]合成了一系列具有相似纳米颗粒形态和比表面积的钙钛矿 AMnO_3 ($A = \text{Ca}, \text{Sr}$ 和 Ba), 研究表明, A 位元素的离子半径变化会导致不同的八面体堆叠,随着离子半径的增加(Ca、到

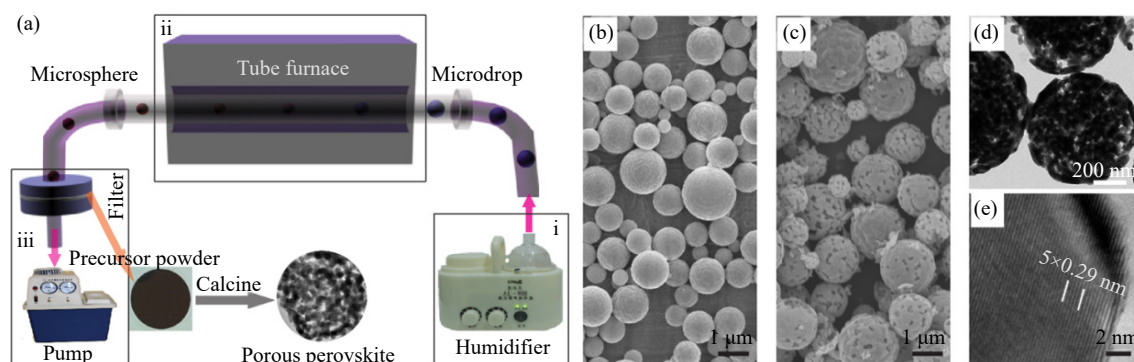


图 11 (a) 介孔 $\text{LaMnO}_{3+\delta}$ 的合成过程, (b) LaMnO_3 前体 SEM 图, (c~e) 介孔 $\text{LaMnO}_{3+\delta}$ 产物 SEM, TEM 和 HRTEM 图像^[105]

Fig.11 (a) Synthesis procedure of the mesoporous $\text{LaMnO}_{3+\delta}$, (b) SEM image of the LaMnO_3 precursor, and (c~e) SEM, TEM, and HRTEM images of the mesoporous $\text{LaMnO}_{3+\delta}$ product^[105]

Sr 到 Ba), 钙钛矿 AMnO_3 发生从正交结构到六方结构的相变(图 12). CaMnO_3 呈正交结构, 由共角八面体组成; SrMnO_3 含面共享和角共享八面体, 交替以立方和六方形式堆叠; BaMnO_3 具有六方结构, 仅含有共面八面体. 具有立方和六方混合堆叠构型的 SrMnO_3 表现出最好的 ORR 催化活性: 半波电位 $\text{SrMnO}_3(0.81 \text{ V}) >$ 半波电位 $\text{CaMnO}_3(0.78 \text{ V}) >$ 半波电位 $\text{BaMnO}_3(0.74 \text{ V})$, 作为 ZABs 催化剂, SrMnO_3 显示出与 Pt/C 相当的峰值功率密度 ($\sim 233 \text{ mW} \cdot \text{cm}^{-2}$), 以及 400 h 的充放电循环稳定性.

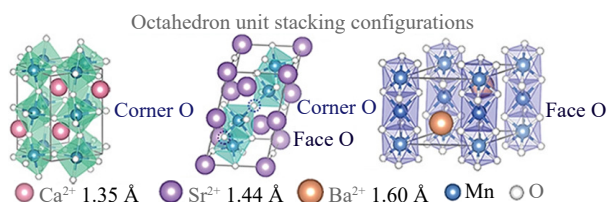


图 12 不同的八面体堆叠结构^[107]

Fig.12 Different octahedron stacking configurations^[107]

钙钛矿的 B 位原子常常采用 Fe、Co、Ni 和 Mn 等其他过渡金属进行部分取代, 用于调控它们的 OER 电催化性能. Hua 等^[108] 的研究表明, 在 $\text{PrBaMn}_2\text{O}_{5+\delta}$ 双钙钛矿中引入适量的 Fe, 能使 B 位阳离子达到高价态和最佳的 e_g 轨道填充, 有助于获得更好的 ORR/OER 电催化性能. Wang 等^[109] 报道了一系列 Mn 掺杂的 $\text{La}_{0.8}\text{Sr}_{0.2}\text{Co}_{1-x}\text{Mn}_x\text{O}_3$ 钙钛矿, 其中 $\text{La}_{0.8}\text{Sr}_{0.2}\text{Co}_{0.4}\text{Mn}_{0.6}\text{O}_3$ 用作 ZABs 的阴极电催化剂时, 比 Pt/C 具有更好的性能和循环耐久性, 其优异活性归因于掺杂导致的 B 位阳离子化学价的变化, 其 $\text{Co}^{3+}/\text{Co}^{2+}$ 比值满足 e_g 占据接近 1 的原则. 非金属元素的掺杂, 特别是磷, 已被证明可有效提高碱性条件下钙钛矿氧化物的 ORR 性能, 例如, Shen 等^[110] 以金属硝酸盐、醋酸盐和 $\text{NH}_4\text{H}_2\text{PO}_4$ 为原料, 采用溶胶-凝胶法制备了磷掺杂的 $\text{La}_{0.8}\text{Sr}_{0.2}\text{MnO}_{3-\delta}$, 其结构

中 5% (原子数分数) 的磷的存在增加了其比表面积并增强了其对含氧中间体的吸附性, 如图 13 (编号中 P 后数字代表 P 的掺杂量) 所示未掺杂的 Mn 2p 3/2 和 Mn 2p 1/2 的特征峰之间的分离距离约为 11.7 eV; 随着 P 掺杂含量的增加, 两个峰的位置逐渐向更高的结合能移动表明在更高的掺杂含量下 Mn 的氧化态增加, 材料内新增了 Mn^{3+} . 相比于未掺杂的材料, Mn 的这种混合价态促进电荷转移到吸附氧的过程, 从而通过快速氧化还原对实现高 ORR 活性, 起始电位为 0.93 V.

提高钙钛矿催化性能的另一方法是引入氧空位. 理想的 ABO_3 钙钛矿结构在其 A 位和 B 位包含等量的阳离子 (即 A/B 阳离子比=1). 但是, 在许多情况下, 当 A/B 阳离子比显著偏离 1 时, 钙钛矿晶格结构仍然可以稳定, 这是由于额外氧空位的存在. Mefford 等^[111] 指出, $\text{La}_{1-x}\text{Sr}_x\text{CoO}_{3-\delta}$ 钙钛矿中更多的氧空位使 Co—O 键更强共价性, 提高了 OER 活性. Gui 等^[112] 设计了一种 $\text{Ce}_{0.9}\text{Gd}_{0.1}\text{O}_{2-\delta}$ 修饰 ($\text{Pr}_{0.5}\text{Ba}_{0.5}$) $\text{CoO}_{3-\delta}$ 钙钛矿复合催化剂, 与原始 ($\text{Pr}_{0.5}\text{Ba}_{0.5}$) $\text{CoO}_{3-\delta}$ 催化剂相比, 更多的表面氧空位使其具有更优异的双功能活性以及耐久性. Yan 等^[113] 发现引入 A 位阳离子缺陷能够显著提高 $\text{LaFeO}_3(\text{LF}, \text{L}$ 后数字代表 La 的含量) 的 ORR 和 OER 电催化活性, 其活性的提高可归因于表面氧空位和少量 Fe^{4+} 物质的产生. 从图 14 (J : 电流密度) 可以看出, 在 1.63 V 时, A 位阳离子缺乏的 $\text{La}_{1-x}\text{FeO}_{3-\delta}$ 催化剂比原始 LF 催化剂具有更好的质量活性和比活性, $\text{L}_{0.95}\text{F}$ 的 Tafel 斜率最小.

高导电性对于提高钙钛矿的 ORR/OER 电催化性能至关重要. 大多数钙钛矿导电性较差, 将其与高导电碳材料 (如碳管、石墨烯) 复合是一有效策略. 例如, Guo 等^[114] 报道了一种由 ($\text{PrBa}_{0.5}\text{Sr}_{0.5}$) $_{0.95}\text{Co}_{1.5}\text{Fe}_{0.5}\text{O}_{5+\delta}$ 和 多孔氮掺杂石墨烯复合的 ORR/OER

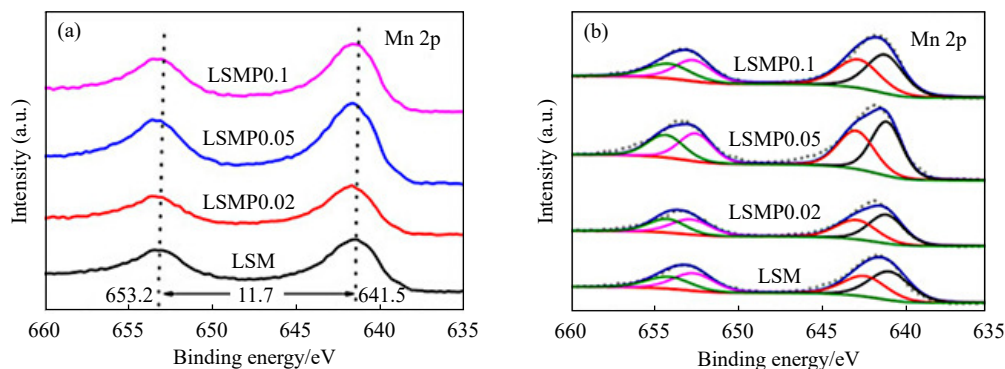


图 13 (a) LSM、LSMP0.02、LSMP0.05 和 LSMP0.1 的 Mn 2p XPS 光谱; (b) LSM、LSMP0.02、LSMP0.05 和 LSMP0.1 的解析 Mn 2p XPS 光谱^[110]
Fig.13 (a) Mn 2p XPS spectra for LSM, LSMP0.02, LSMP0.05, and LSMP0.1 and (b) resolved Mn 2p XPS spectra for LSM, LSMP0.02, LSMP0.05, and LSMP0.1^[110]

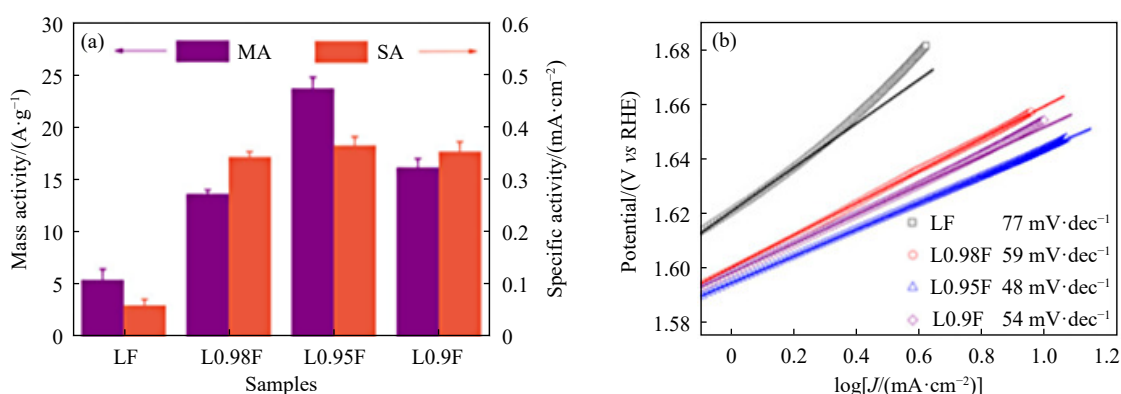


图 14 (a) LF、L_{0.98}F、L_{0.95}F 和 L_{0.9}F 催化剂在 1.63 V 时的 OER 质量活性 (MA) 和比活性 (SA); (b) LF、L_{0.98}F、L_{0.95}F 和 L_{0.9}F 催化剂的 Tafel 图^[113]
Fig.14 (a) OER mass activity (MA) and specific activity (SA) of the LF, L_{0.98}F, L_{0.95}F, and L_{0.9}F catalysts at 1.63 V; (b) Tafel plots of the LF, L_{0.98}F, L_{0.95}F, and L_{0.9}F catalysts^[113]

催化剂; Hu 等^[115] 通过水热法制备了 LaNiO₃ 纳米棒/石墨烯复合催化剂, 作为 ZABs 的双功能催化剂, 充放电的循环性能和稳定性显著高于商用 Pt/C. Prabu 等^[116] 将一维钙钛矿 LaTi_{0.65}Fe_{0.35}O_{3-δ} (LTFO) 纳米颗粒嵌入在碳纳米棒表面和内部, 凭借高表面积、高氮官能团的、高度石墨化碳的存在以及高活性 LTFO 中心在高导电碳纳米棒上的良好分散, 其表现出了良好的双功能活性 ($\Delta E=1.1$ V). 表 3 总结了最近报导的部分钙钛矿双功能 ORR/OER 催化剂的性能.

4 总结及展望

作为一种新型的储能技术, 可充放电锌-空气电池 (Zinc-air batteries, ZABs) 因其高的能量密度、高安全性和低成本, 被认为具有广阔的应用前景. 但是, 若要实现锌空气电池的商业化应用, 尚有大量的科学问题有待解决. 其中, ORR 及 OER 的缓慢反应动力学制约了 ZABs 的充放电性能, 因此, 目前迫切需要开发一种高活性, 高稳定性的催化剂. 本文对最近报导的具有 ORR 和 OER 双功能活

性的过渡金属氧化物电催化剂的研究进展进行了总结并对其进行如下展望.

(1) 要对 ORR 和 OER 的反应过程有更深入的了解, 包括反应途径、活性位点的识别、界面行为等方面, 同时需要开发更先进的表征方法, 相关催化机制的日益清晰将对新型催化剂的开发带来更多帮助.

(2) 双功能催化剂在 ZABs 工作时的位点失活问题需要格外关注, 特别是 ORR 活性位点在 OER 条件下易发生不可逆的损坏, 这往往给材料的复合设计带来困难. 目前已有新的电池设计的报道, 将 ORR 和 OER 解耦, 分别在放电电极和充电电极上各自发生, 目的就是避免上述问题.

(3) 碳复合仍然是目前双功能催化剂主要的制备策略之一, 一是因为碳材料可以增加电化学面积, 并提高导电性, 同时碳材料也容易形成多孔结构来加快传质; 此外, 碳基材料, 尤其是碳基单原子材料本身有较高的 ORR 活性, 将其与 OER 活性物质复合后容易展现出双功能特性. 但是, 随之而来的, 碳在 OER 条件下的氧化和 ORR 位点失效

表3 一些钙钛矿型电催化剂的双功能性能

Table 3 Bifunctional properties of some perovskite-type electrocatalysts

Reference	Electrocatalyst	Loading/ (mg·cm ⁻²)	$\Delta E/V$	$E_{1/2}/V(\text{vs RHE})$	$E_{10}/V(\text{vs RHE})$	Electrolyte
[117]	CLSR	0.7	0.92	0.8	1.72	0.1 mol·L ⁻¹ KOH
[118]	L0.95F	0.232	1.06	0.38	1.64	0.1 mol·L ⁻¹ KOH
[119]	NSC@IGnP	0.25	1.02	0.64	1.66	0.1 mol·L ⁻¹ KOH
[120]	mesoporous LSCO		1.11	0.72	1.83	0.1 mol·L ⁻¹ KOH
[121]	urchin-like LSM	0.655	1.65	0.59	2.24	0.1 mol·L ⁻¹ KOH
[116]	LTFO-C		1.05	0.72	1.77	0.1 mol·L ⁻¹ KOH
[122]	LaCoO ₃	0.051	1.1	0.64	1.74	0.1 mol·L ⁻¹ KOH
[123]	LaNi _{0.8} Fe _{0.2} O ₃	0.2	1.09	0.4	1.49	0.1 mol·L ⁻¹ KOH
[124]	BaFe _{0.8} Co _{0.2} O _{2.09} (OH) _{0.78}	0.3	1.005	0.675	1.68	0.1 mol·L ⁻¹ KOH
[125]	LC5N5	0.25	0.96	0.67	1.63	0.1 mol·L ⁻¹ KOH
[126]	PBSCF-NF		0.84	0.69	1.53	0.1 mol·L ⁻¹ KOH
[127]	S5.84%-LCO		0.89	0.704	1.594	0.1 mol·L ⁻¹ KOH
[128]	NCNT-660	0.21	0.88	0.74	1.62	1 mol·L ⁻¹ KOH
[129]	LSCF-6482	1.8	0.83	0.82	1.65	0.1 mol·L ⁻¹ KOH
[130]	La0.3-5582	0.639	1.01	0.55	1.56	0.1 mol·L ⁻¹ KOH
[131]	LSMF	0.458	1.11	0.73	1.84	0.1 mol·L ⁻¹ KOH
[132]	LO-NF-NCNTs-1.0	0.4	0.938	0.772	1.71	0.1 mol·L ⁻¹ KOH
[133]	SSC-HG	0.796	0.84	0.79	1.63	0.1 mol·L ⁻¹ KOH
[134]	nsLaNiO ₃ /NC	0.05	1.02	0.64	1.66	0.1 mol·L ⁻¹ KOH
[135]	LSMI	0.2	0.94	0.73	1.67	0.1 mol·L ⁻¹ KOH
[136]	CMO/S-300	0.1	0.94	0.76	1.77	0.1 mol·L ⁻¹ KOH
[137]	LFP-5	0.255	1.03	0.66	1.61	0.1 mol·L ⁻¹ KOH
[138]	BSCF/NiFe-25	0.4	0.785	0.78	1.574	0.1 mol·L ⁻¹ KOH

问题需要进一步解决。

(4)总的来说,由于 ORR 和 OER 的四电子特点,目前报道的各类催化剂仍然具有很高的过电势,导致可充放电 ZABs 能量效率仍然较低,这极大限制了该类电池的广泛应用,因此,发现新的高活性催化剂十分必要且任务艰巨,人工智能、机器学习等大数据技术未来有望带来新的机遇。

参 考 文 献

- [1] Zhou T P, Zhang N, Wu C Z, et al. Surface/interface nanoengineering for rechargeable Zn-air batteries. *Energy Environ Sci*, 2020, 13(4): 1132
- [2] Pan J, Xu Y Y, Yang H, et al. Advanced architectures and relatives of air electrodes in Zn-air batteries. *Adv Sci*, 2018, 5(4): 1700691
- [3] Park M, Zhang X C, Chung M, et al. A review of conduction phenomena in Li-ion batteries. *J Power Sources*, 2010, 195(24): 7904
- [4] Ye F, Liao K M, Ran R, et al. Recent advances in filler engineering of polymer electrolytes for solid-state Li-ion batteries: A review. *Energy Fuels*, 2020, 34(8): 9189
- [5] Kim H J, Krishna T, Zeb K, et al. A comprehensive review of Li-ion battery materials and their recycling techniques. *Electronics*, 2020, 9(7): 1161
- [6] Wang Y J, Fan H B, Ignaszak A, et al. Compositing doped-carbon with metals, non-metals, metal oxides, metal nitrides and other materials to form bifunctional electrocatalysts to enhance metal-air battery oxygen reduction and evolution reactions. *Chem Eng J*, 2018, 348: 416
- [7] Zhang D, Zhao H P, Liang F, et al. Nanostructured arrays for metal-ion battery and metal-air battery applications. *J Power Sources*, 2021, 493: 229722
- [8] Fu J, Cano Z P, Park M G, et al. Electrically rechargeable zinc-air batteries: Progress, challenges, and perspectives. *Adv Mater*, 2017, 29(7): 1604685
- [9] Zhang Y G, Deng Y P, Wang J Y, et al. Recent progress on flexible Zn-air batteries. *Energy Storage Mater*, 2021, 35: 538
- [10] Caramia V, Bozzini B. Materials science aspects of zinc-air

- batteries: A review. *Mater Renew Sustain Energy*, 2014, 3(2): 1
- [11] Lee J S, Kim S T, Cao R G, et al. Metal-air batteries with high energy density: Li-air versus Zn-air. *Adv Energy Mater*, 2011, 1(1): 34
- [12] Wang H F, Tang C, Zhang Q. A review of precious-metal-free bifunctional oxygen electrocatalysts: Rational design and applications in Zn-Air batteries. *Adv Funct Mater*, 2018, 28(46): 1803329
- [13] Yu X X, Zhou T P, Ge J K, et al. Recent advances on the modulation of electrocatalysts based on transition metal nitrides for the rechargeable Zn-air battery. *ACS Mater Lett*, 2020, 2(11): 1423
- [14] Ren S S, Duan X D, Liang S, et al. Bifunctional electrocatalysts for Zn-air batteries: Recent developments and future perspectives. *J Mater Chem A*, 2020, 8(13): 6144
- [15] Tang X N, Wei Y H, Zhai W J, et al. Carbon nanocage with maximum utilization of atomically dispersed iron as efficient oxygen electroreduction nanoreactor. *Adv Mater*, 2023, 35(5): 2208942
- [16] Huang B Y, Huang S H, Lu C B, et al. Decrypting the influence of axial coordination on the electronic microenvironment of co-N₅ site for enhanced electrocatalytic reaction. *CCS Chem*, 2023, 5(8): 1876
- [17] Chen J D, Huang B Y, Cao R, et al. Steering local electronic configuration of Fe-N-C-based coupling catalysts via ligand engineering for efficient oxygen electroreduction. *Adv Funct Mater*, 2023, 33(4): 2209315
- [18] Li L B, Yuan K, Chen Y W. Breaking the scaling relationship limit: From single-atom to dual-atom catalysts. *Acc Mater Res*, 2022, 3(6): 584
- [19] Lu X F, Chen Y, Wang S B, et al. Interfacing manganese oxide and cobalt in porous graphitic carbon polyhedrons boosts oxygen electrocatalysis for Zn-air batteries. *Adv Mater*, 2019, 31(39): 1902339
- [20] Mao L Q, Zhang D, Sotomura T, et al. Mechanistic study of the reduction of oxygen in air electrode with manganese oxides as electrocatalysts. *Electrochim Acta*, 2003, 48(8): 1015
- [21] Roche I, Chaînet E, Chatenet M, et al. Carbon-supported manganese oxide nanoparticles as electrocatalysts for the oxygen reduction reaction (ORR) in alkaline medium: physical characterizations and ORR mechanism. *J Phys Chem C*, 2007, 111(3): 1434
- [22] Jiao F, Frei H. Nanostructured cobalt oxide clusters in mesoporous silica as efficient oxygen-evolving catalysts. *Angew Chem Int Ed*, 2009, 121(10): 1873
- [23] Jiao F, Frei H. Nanostructured manganese oxide clusters supported on mesoporous silica as efficient oxygen-evolving catalysts. *Chem Commun*, 2010, 46(17): 2920
- [24] Meng Y T, Song W Q, Huang H, et al. Structure-property relationship of bifunctional MnO₂ nanostructures: Highly efficient, ultra-stable electrochemical water oxidation and oxygen reduction reaction catalysts identified in alkaline media. *J Am Chem Soc*, 2014, 136(32): 11452
- [25] Cheng F Y, Su Y, Liang J, et al. MnO₂-based nanostructures as catalysts for electrochemical oxygen reduction in alkaline media. *Chem Mater*, 2010, 22(3): 898
- [26] Yan G B, Lian Y B, Gu Y D, et al. Phase and morphology transformation of MnO₂ induced by ionic liquids toward efficient water oxidation. *ACS Catal*, 2018, 8(11): 10137
- [27] Casas-Cabanas M, Binotto G, Larcher D, et al. Defect chemistry and catalytic activity of nanosized Co₃O₄. *Chem Mater*, 2009, 21(9): 1939
- [28] Zhang X, Yu P, Wang D L, et al. Controllable synthesis of α -MnO₂ nanostructures and phase transformation to β -MnO₂ microcrystals by hydrothermal crystallization. *J Nanosci Nanotech*, 2010, 10(2): 898
- [29] Worku A K, Ayele D W, Habtu N G, et al. Recent progress in MnO₂-based oxygen electrocatalysts for rechargeable zinc-air batteries. *Mater Today Sustain*, 2021, 13: 100072
- [30] Ding Y S, Shen X F, Sithambaram S, et al. Synthesis and catalytic activity of cryptomelane-type manganese dioxide nanomaterials produced by a novel solvent-free method. *Chem Mater*, 2005, 17(21): 5382
- [31] Zhou M, Zhang X, Wei J M, et al. Morphology-controlled synthesis and novel microwave absorption properties of hollow urchinlike α -MnO₂ nanostructures. *J Phys Chem C*, 2011, 115(5): 1398
- [32] Bôas N V, Junior J S, Varanda L C, et al. Bismuth and cerium doped cryptomelane-type manganese dioxide nanorods as bifunctional catalysts for rechargeable alkaline metal-air batteries. *Appl Catal B*, 2019, 258(C): 118014
- [33] Song S D, Li W J, Deng Y P, et al. TiC supported amorphous MnO_x as highly efficient bifunctional electrocatalyst for corrosion resistant oxygen electrode of Zn-air batteries. *Nano Energy*, 2020, 67: 104208
- [34] Pandey J, Hua B, Ng W, et al. Developing hierarchically porous MnO_x/NC hybrid nanorods for oxygen reduction and evolution catalysis. *Green Chem*, 2017, 19(12): 2793
- [35] Chen S, Shu X X, Wang H S, et al. Thermally driven phase transition of manganese oxide on carbon cloth for enhancing the performance of flexible all-solid-state zinc-air batteries. *J Mater Chem A*, 2019, 7(34): 19719
- [36] Ji D X, Sun J G, Tian L D, et al. Engineering of the heterointerface of porous carbon nanofiber-supported nickel and manganese oxide nanoparticle for highly efficient bifunctional oxygen catalysis. *Adv Funct Mater*, 2020, 30(13): 1910568
- [37] Chen Y N, Guo Y B, Cui H J, et al. Bifunctional electrocatalysts of MOF-derived Co-N/C on bamboo-like MnO nanowires for high-performance liquid- and solid-state Zn-air batteries. *J Mater Chem A*, 2018, 6(20): 9716
- [38] Xing X L, Liu R J, Cao K C, et al. Manganese vanadium oxide-N-doped reduced graphene oxide composites as oxygen

- reduction and oxygen evolution electrocatalysts. *ACS Appl Mater Interfaces*, 2018, 10(51): 44511
- [39] Selvakumar K, Kumar S M S, Thangamuthu R, et al. 2D and 3D silica-template-derived MnO₂ electrocatalysts towards enhanced oxygen evolution and oxygen reduction activity. *ChemElectroChem*, 2018, 5(24): 3980
- [40] He J K, Wang M C, Wang W B, et al. Hierarchical mesoporous NiO/MnO₂@PANI core-shell microspheres, highly efficient and stable bifunctional electrocatalysts for oxygen evolution and reduction reactions. *ACS Appl Mater Interfaces*, 2017, 9(49): 42676
- [41] Wang P C, Lin Y Q, Wan L, et al. Construction of a Janus MnO₂-NiFe electrode via selective electrodeposition strategy as a high-performance bifunctional electrocatalyst for rechargeable zinc-air batteries. *ACS Appl Mater Interfaces*, 2019, 11(41): 37701
- [42] Cheng Y, Dou S, Saunders M, et al. A class of transition metal-oxide@MnO_x core-shell structured oxygen electrocatalysts for reversible O₂ reduction and evolution reactions. *J Mater Chem A*, 2016, 4(36): 13881
- [43] Xu Y F, Chen Y, Xu G L, et al. RuO₂ nanoparticles supported on MnO₂ nanorods as high efficient bifunctional electrocatalyst of lithium-oxygen battery. *Nano Energy*, 2016, 28: 63
- [44] Maji B, Das A, Barik B, et al. Cation substitution effects (Mn, Ni, and Zn) on ZIF-67 derived spinel modified with 3DGO for the detection of NO₂ gas with high sensitivity and selectivity. *Environ Sci Nano*, <https://doi.org/10.1039/D3EN00205E>
- [45] Wei C, Feng Z X, Scherer G G, et al. Cations in octahedral sites: A descriptor for oxygen electrocatalysis on transition-metal spinels. *Adv Mater*, 2017, 29(23): 1606800
- [46] Pan J, Tian X L, Zaman S, et al. Recent progress on transition metal oxides as bifunctional catalysts for lithium-air and zinc-air batteries. *Batter Supercaps*, 2019, 2(4): 336
- [47] Davari E, Ivey D G. Bifunctional electrocatalysts for Zn-air batteries. *Sustainable Energy Fuels*, 2018, 2(1): 39
- [48] Zhou Y, Sun S N, Wei C, et al. Significance of engineering the octahedral units to promote the oxygen evolution reaction of spinel oxides. *Adv Mater*, 2019, 31(41): 1902509
- [49] Zhao Q, Yan Z H, Chen C C, et al. Spinel: Controlled preparation, oxygen reduction/evolution reaction application, and beyond. *Chem Rev*, 2017, 117(15): 10121
- [50] Dai Y W, Yu J E, Ni M, et al. Rational design of spinel oxides as bifunctional oxygen electrocatalysts for rechargeable Zn-air batteries. *Chem Phys Rev*, 2020, 1(1): 011303
- [51] Sun S N, Sun Y M, Zhou Y, et al. Switch of the rate-determining step of water oxidation by spin-selected electron transfer in spinel oxides. *Chem Mater*, 2019, 31(19): 8106
- [52] Prabu M, Ramakrishnan P, Shanmugam S. CoMn₂O₄ nanoparticles anchored on nitrogen-doped graphene nanosheets as bifunctional electrocatalyst for rechargeable zinc-air battery. *Electrochem Commun*, 2014, 41: 59
- [53] Li S S, Chen W H, Pan H Z, et al. FeCo alloy nanoparticles coated by an ultrathin N-doped carbon layer and encapsulated in carbon nanotubes as a highly efficient bifunctional air electrode for rechargeable Zn-air batteries. *ACS Sustainable Chem Eng*, 2019, 7(9): 8530
- [54] Su H, Wang X T, Hu J X, et al. Co-Mn spinel supported self-catalysis induced N-doped carbon nanotubes with high efficiency electron transport channels for zinc-air batteries. *J Mater Chem A*, 2019, 7(39): 22307
- [55] Zhang Y Q, Li M, Hua B, et al. A strongly cooperative spinel nanohybrid as an efficient bifunctional oxygen electrocatalyst for oxygen reduction reaction and oxygen evolution reaction. *Appl Catal B*, 2018, 236: 413
- [56] Mu C, Mao J, Guo J X, et al. Rational design of spinel cobalt vanadate oxide Co₂VO₄ for superior electrocatalysis. *Adv Mater*, 2020, 32(10): 1907168
- [57] Liu Z Q, Cheng H, Li N, et al. ZnCo₂O₄ quantum dots anchored on nitrogen-doped carbon nanotubes as reversible oxygen reduction/evolution electrocatalysts. *Adv Mater*, 2016, 28(19): 3777
- [58] Jiang Y, Deng Y P, Fu J, et al. Interpenetrating triphase cobalt-based nanocomposites as efficient bifunctional oxygen electrocatalysts for long-lasting rechargeable Zn-air batteries. *Adv Energy Mater*, 2018, 8(15): 1702900
- [59] Rao Y, Chen S, Yue Q, et al. Optimizing the spin states of mesoporous Co₃O₄ nanorods through vanadium doping for long-lasting and flexible rechargeable Zn-air batteries. *ACS Catal*, 2021, 11(13): 8097
- [60] Wang Z P, Huang J H, Wang L, et al. Cation-tuning induced d-band center modulation on co-based spinel oxide for oxygen reduction/evolution reaction. *Angew Chem Int Ed*, 2022, 61(16): e202114696
- [61] Liu W J, Bao J, Xu L, et al. NiCo₂O₄ ultrathin nanosheets with oxygen vacancies as bifunctional electrocatalysts for Zn-air battery. *Appl Surf Sci*, 2019, 478: 552
- [62] Zhang Z M, Liang X L, Li J F, et al. Interfacial engineering of NiO/NiCo₂O₄ porous nanofibers as efficient bifunctional catalysts for rechargeable zinc-air batteries. *ACS Appl Mater Interfaces*, 2020, 12(19): 21661
- [63] Li J, Lu S Q, Huang H L, et al. ZIF-67 as continuous self-sacrifice template derived NiCo₂O₄/Co, N-CNTs nanocages as efficient bifunctional electrocatalysts for rechargeable Zn-air batteries. *ACS Sustainable Chem Eng*, 2018, 6(8): 10021
- [64] Li Z S, Li B L, Chen J M, et al. Spinel NiCo₂O₄ 3-D nanoflowers supported on graphene nanosheets as efficient electrocatalyst for oxygen evolution reaction. *Int J Hydrog Energy*, 2019, 44(31): 16120
- [65] Jiang Z Q, Jiang Z J, Maiyalagan T, et al. Cobalt oxide-coated N- and B-doped graphene hollow spheres as bifunctional electrocatalysts for oxygen reduction and oxygen evolution reactions. *J Mater Chem A*, 2016, 4(16): 5877
- [66] Li G, Wang X L, Fu J, et al. Pomegranate-inspired design of

- highly active and durable bifunctional electrocatalysts for rechargeable metal-air batteries. *Angew Chem Int Ed*, 2016, 55(16): 4977
- [67] Chen X, Yan Z H, Yu M, et al. Spinel oxide nanoparticles embedded in nitrogen-doped carbon nanofibers as a robust and self-standing bifunctional oxygen cathode for Zn-air batteries. *J Mater Chem A*, 2019, 7: 24868
- [68] Abirami M, Hwang S M, Yang J C, et al. A metal-organic framework derived porous cobalt manganese oxide bifunctional electrocatalyst for hybrid Na-air/seawater batteries. *ACS Appl Mater Interfaces*, 2016, 8(48): 32778
- [69] Feng X T, Jiao Q Z, Cui H R, et al. One-pot synthesis of NiCo₂S₄ hollow spheres via sequential ion-exchange as an enhanced oxygen bifunctional electrocatalyst in alkaline solution. *ACS Appl Mater Interfaces*, 2018, 10(35): 29521
- [70] Si C H, Zhang Y L, Zhang C Q, et al. Mesoporous nanostructured spinel-type MFe₂O₄ (M = Co, Mn, Ni) oxides as efficient bifunctional electrocatalysts towards oxygen reduction and oxygen evolution. *Electrochim Acta*, 2017, 245: 829
- [71] Ma N, Jia Y A, Yang X F, et al. Seaweed biomass derived (Ni, Co)/CNT nanoaerogels: Efficient bifunctional electrocatalysts for oxygen evolution and reduction reactions. *J Mater Chem A*, 2016, 4(17): 6376.
- [72] Guan J L, Zhang Z P, Ji J, et al. Hydrothermal synthesis of highly dispersed Co₃O₄ nanoparticles on biomass-derived nitrogen-doped hierarchically porous carbon networks as an efficient bifunctional electrocatalyst for oxygen reduction and evolution reactions. *ACS Appl Mater Interfaces*, 2017, 9(36): 30662
- [73] Ma L, Zhou H, Sun Y, et al. Nanosheet-structured NiCoO₂/carbon nanotubes hybrid composite as a novel bifunctional oxygen electrocatalyst. *Electrochim Acta*, 2017, 252: 338
- [74] Pendashteh A, Palma J, Anderson M, et al. NiCoMnO₄ nanoparticles on N-doped graphene: Highly efficient bifunctional electrocatalyst for oxygen reduction/evolution reactions. *Appl Catal B*, 2017, 201: 241
- [75] Liang Y Y, Li Y G, Wang H L, et al. Co₃O₄ nanocrystals on graphene as a synergistic catalyst for oxygen reduction reaction. *Nat Mater*, 2011, 10(10): 780
- [76] Liu Q, Jin J T, Zhang J Y. NiCo₂S₄@graphene as a bifunctional electrocatalyst for oxygen reduction and evolution reactions. *ACS Appl Mater Interfaces*, 2013, 5(11): 5002
- [77] Han X P, Wu X Y, Zhong C, et al. NiCo₂S₄ nanocrystals anchored on nitrogen-doped carbon nanotubes as a highly efficient bifunctional electrocatalyst for rechargeable zinc-air batteries. *Nano Energy*, 2017, 31: 541
- [78] Zhou J Q, Wang M F, Qian T, et al. Porous yolk-shell microspheres as N-doped carbon matrix for motivating the oxygen reduction activity of oxygen evolution oriented materials. *Nanotechnology*, 2017, 28(36): 365403
- [79] Bai Z Y, Heng J M, Zhang Q, et al. Rational design of dodecahedral MnCo₂O_{4.5} hollowed-out nanocages as efficient bifunctional electrocatalysts for oxygen reduction and evolution. *Adv Energy Mater*, 2018, 8(34): 1802390
- [80] Lee D U, Park M G, Cano Z P, et al. Hierarchical core-shell nickel cobaltite chestnut-like structures as bifunctional electrocatalyst for rechargeable metal-air batteries. *ChemSusChem*, 2018, 11(2): 406
- [81] Maiyalagan T, Jarvis K A, Therese S, et al. Spinel-type lithium cobalt oxide as a bifunctional electrocatalyst for the oxygen evolution and oxygen reduction reactions. *Nat Commun*, 2014, 5: 3949
- [82] Li Y X, Yin J, An L, et al. Metallic CuCo₂S₄ nanosheets of atomic thickness as efficient bifunctional electrocatalysts for portable, flexible Zn-air batteries. *Nanoscale*, 2018, 10(14): 6581
- [83] Zhou Y, Du Y H, Xi S B, et al. Spinel manganese ferrites for oxygen electrocatalysis: Effect of Mn valency and occupation site. *Electrocatalysis*, 2018, 9(3): 287
- [84] Song W Q, Ren Z, Chen S Y, et al. Ni- and Mn-promoted mesoporous Co₃O₄: A stable bifunctional catalyst with surface-structure-dependent activity for oxygen reduction reaction and oxygen evolution reaction. *ACS Appl Mater Interfaces*, 2016, 8(32): 20802
- [85] Hu T J, Wang Y, Zhang L N, et al. Facile synthesis of PdO-doped Co₃O₄ nanoparticles as an efficient bifunctional oxygen electrocatalyst. *Appl Catal B*, 2019, 243: 175
- [86] Li H C, Zhang Y J, Hu X, et al. Metal-organic framework templated Pd@PdO-Co₃O₄ nanocubes as an efficient bifunctional oxygen electrocatalyst. *Adv Energy Mater*, 2018, 8(11): 1702734
- [87] Wang C W, Zhao Z, Li X F, et al. Three-dimensional framework of graphene nanomeshes shell/Co₃O₄ synthesized as superior bifunctional electrocatalyst for zinc-air batteries. *ACS Appl Mater Interfaces*, 2017, 9(47): 41273
- [88] Wang X J, Li Y, Jin T, et al. Electrospun thin-walled CuCo₂O₄@C nanotubes as bifunctional oxygen electrocatalysts for rechargeable Zn-air batteries. *Nano Lett*, 2017, 17(12): 7989
- [89] Liang Y X, Gong Q J, Sun X L, et al. Rational fabrication of thin-layered NiCo₂S₄ loaded graphene as bifunctional non-oxide catalyst for rechargeable zinc-air batteries. *Electrochim Acta*, 2020, 342: 136108
- [90] Liu J N, Li B Q, Zhao C X, et al. A composite bifunctional oxygen electrocatalyst for high-performance rechargeable zinc-air batteries. *ChemSusChem*, 2020, 13(6): 1529
- [91] Zhu Y L, Zhou W, Shao Z P. Perovskite/carbon composites: Applications in oxygen electrocatalysis. *Small*, 2017, 13(12): 1603793
- [92] Yu J, Ran R, Zhong Y J, et al. Advances in porous perovskites: Synthesis and electrocatalytic performance in fuel cells and metal-air batteries. *Energy Environ Mater*, 2020, 3(2): 121
- [93] Xu X M, Wang W, Zhou W, et al. Recent advances in novel nanostructuring methods of perovskite electrocatalysts for energy-related applications. *Small Meth*, 2018, 2(7): 1800071

- [94] Yoo J S, Rong X, Liu Y S, et al. Role of lattice oxygen participation in understanding trends in the oxygen evolution reaction on perovskites. *ACS Catal*, 2018, 8(5): 4628
- [95] Pan Y L, Xu X M, Zhong Y J, et al. Direct evidence of boosted oxygen evolution over perovskite by enhanced lattice oxygen participation. *Nat Commun*, 2020, 11: 2002
- [96] Song J J, Wei C, Huang Z F, et al. A review on fundamentals for designing oxygen evolution electrocatalysts. *Chem Soc Rev*, 2020, 49(7): 2196
- [97] Suntivich J, Gasteiger H A, Yabuuchi N, et al. Design principles for oxygen-reduction activity on perovskite oxide catalysts for fuel cells and metal-air batteries. *Nat Chem*, 2011, 3(7): 546
- [98] Suntivich J, May K J, Gasteiger H A, et al. A perovskite oxide optimized for oxygen evolution catalysis from molecular orbital principles. *Science*, 2011, 334(6061): 1383
- [99] Lu F L, Sui J, Su J M, et al. Hollow spherical $\text{La}_{0.8}\text{Sr}_{0.2}\text{MnO}_3$ perovskite oxide with enhanced catalytic activities for the oxygen reduction reaction. *J Power Sources*, 2014, 271: 55
- [100] Yang Y S, Zhou W, Liu R C, et al. *In situ* tetraethoxysilane-templated porous $\text{Ba}_{0.5}\text{Sr}_{0.5}\text{Co}_{0.8}\text{Fe}_{0.2}\text{O}_{3-\delta}$ perovskite for the oxygen evolution reaction. *ChemElectroChem*, 2015, 2(2): 200
- [101] Lu F L, Wang Y R, Jin C, et al. Microporous $\text{La}_{0.8}\text{Sr}_{0.2}\text{MnO}_3$ perovskite nanorods as efficient electrocatalysts for lithium-air battery. *J Power Sources*, 2015, 293: 726
- [102] Xu J J, Wang Z L, Xu D, et al. 3D ordered macroporous LaFeO_3 as efficient electrocatalyst for Li-O₂ batteries with enhanced rate capability and cyclic performance. *Energy Environ Sci*, 2014, 7(7): 2213
- [103] Jung J I, Risch M, Park S, et al. Optimizing nanoparticle perovskite for bifunctional oxygen electrocatalysis. *Energy Environ Sci*, 2016, 9(1): 176
- [104] Cai B, Akkiraju K, Mounfield W P III, et al. Solid-state gelation for nanostructured perovskite oxide aerogels. *Chem Mater*, 2019, 31(22): 9422
- [105] Kuai L, Kan E J, Cao W, et al. Mesoporous $\text{LaMnO}_{3+\delta}$ perovskite from spray-pyrolysis with superior performance for oxygen reduction reaction and Zn-air battery. *Nano Energy*, 2018, 43: 81
- [106] Azizi F, Kahoul A, Azizi A. Effect of La doping on the electrochemical activity of double perovskite oxide $\text{Sr}_2\text{FeMoO}_6$ in alkaline medium. *J Alloys Compd*, 2009, 484(1-2): 555
- [107] Zhao C N, Zhang X L, Yu M, et al. Cooperative catalysis toward oxygen reduction reaction under dual coordination environments on intrinsic AMnO_3^- Type perovskites via regulating stacking configurations of coordination units. *Adv Mater*, 2020, 32(50): 2006145
- [108] Hua B, Sun Y F, Li M, et al. Stabilizing double perovskite for effective bifunctional oxygen electrocatalysis in alkaline conditions. *Chem Mater*, 2017, 29(15): 6228
- [109] Wang Q, Xue Y J, Sun S S, et al. $\text{La}_{0.8}\text{Sr}_{0.2}\text{Co}_{1-x}\text{Mn}_x\text{O}_3$ perovskites as efficient bi-functional cathode catalysts for rechargeable zinc-air batteries. *Electrochim Acta*, 2017, 254: 14
- [110] Shen Y J, Zhu Y L, Sunarso J, et al. Frontispiece: New phosphorus-doped perovskite oxide as an oxygen reduction reaction electrocatalyst in an alkaline solution. *Chem A Eur J*, 2018, 24(27): 6950
- [111] Mefford J T, Rong X, Abakumov A M, et al. Water electrolysis on $\text{La}_{1-x}\text{Sr}_x\text{CoO}_{3-\delta}$ perovskite electrocatalysts. *Nat Commun*, 2016, 7(1): 11053
- [112] Gui L Q, Wang Z B, Zhang K, et al. Oxygen vacancies-rich $\text{Ce}_{0.9}\text{Gd}_{0.1}\text{O}_{2-\delta}$ decorated $\text{Pr}_{0.5}\text{Ba}_{0.5}\text{CoO}_{3-\delta}$ bifunctional catalyst for efficient and long-lasting rechargeable Zn-air batteries. *Appl Catal B*, 2020, 266: 118656
- [113] Yan D F, Li Y X, Huo J, et al. Defect chemistry of nonprecious-metal electrocatalysts for oxygen reactions. *Adv Mater*, 2017, 29(48): 1606459
- [114] Chai G L, Qiu K P, Qiao M, et al. Active sites engineering leads to exceptional ORR and OER bifunctionality in P, N Co-doped graphene frameworks. *Energy Environ Sci*, 2017, 10(5): 1186
- [115] Hu J E, Liu Q N, Shi Z W, et al. LaNiO_3 -nanorod/graphene composite as an efficient bi-functional catalyst for zinc-air batteries. *RSC Adv*, 2016, 6(89): 86386
- [116] Prabu M, Ramakrishnan P, Ganesan P, et al. $\text{LaTi}_{0.65}\text{Fe}_{0.35}\text{O}_{3-\delta}$ nanoparticle-decorated nitrogen-doped carbon nanorods as an advanced hierarchical air electrode for rechargeable metal-air batteries. *Nano Energy*, 2015, 15: 92
- [117] Kumar N, Kumar M, Nagaiah T C, et al. Investigation of new B-site-disordered perovskite oxide $\text{CaLaSeRuO}_{6+\delta}$: An efficient oxygen bifunctional electrocatalyst in a highly alkaline medium. *ACS Appl Mater Interfaces*, 2020, 12(8): 9190
- [118] Zhu Y L, Zhou W, Yu J, et al. Enhancing electrocatalytic activity of perovskite oxides by tuning cation deficiency for oxygen reduction and evolution reactions. *Chem Mater*, 2016, 28(6): 1691
- [119] Kim C, Gwon O, Jeon I Y, et al. Cloud-like graphene nanoplatelets on $\text{Nd}_{0.5}\text{Sr}_{0.5}\text{CoO}_{3-\delta}$ nanorods as an efficient bifunctional electrocatalyst for hybrid Li-air batteries. *J Mater Chem A*, 2016, 4(6): 2122
- [120] Zhao Y L, Xu L, Mai L Q, et al. Hierarchical mesoporous perovskite $\text{La}_{0.5}\text{Sr}_{0.5}\text{CoO}_{2.91}$ nanowires with ultrahigh capacity for Li-air batteries. *Proc Natl Acad Sci USA*, 2012, 109(48): 19569
- [121] Jin C, Cao X C, Zhang L Y, et al. Preparation and electrochemical properties of urchin-like $\text{La}_{0.8}\text{Sr}_{0.2}\text{MnO}_3$ perovskite oxide as a bifunctional catalyst for oxygen reduction and oxygen evolution reaction. *J Power Sources*, 2013, 241: 225
- [122] Hardin W G, Mefford J T, Slanac D A, et al. Tuning the electrocatalytic activity of perovskites through active site variation and support interactions. *Chem Mater*, 2014, 26(11): 3368
- [123] Zhang D W, Song Y F, Du Z Z, et al. Active $\text{LaNi}_{1-x}\text{Fe}_x\text{O}_3$ bifunctional catalysts for air cathodes in alkaline media. *J Mater Chem A*, 2015, 3(18): 9421

- [124] Waidha A I, Ni L M, Ali J, et al. Synthesis of bifunctional $\text{BaFe}_{1-x}\text{Co}_x\text{O}_{3-y}\text{-(OH)}_y$ catalysts for the oxygen reduction reaction and oxygen evolution reaction. *J Mater Chem A*, 2020, 8(2): 616
- [125] Wang H Z, Xu W C, Richins S, et al. Polymer-assisted approach to $\text{LaCo}_{1-x}\text{Ni}_x\text{O}_3$ network nanostructures as bifunctional oxygen electrocatalysts. *Electrochim Acta*, 2019, 296: 945
- [126] Bu Y F, Gwon O, Nam G, et al. A highly efficient and robust cation ordered perovskite oxide as a bifunctional catalyst for rechargeable zinc-air batteries. *ACS Nano*, 2017, 11(11): 11594
- [127] Ran J, Wang T, Zhang J, et al. Modulation of electronics of oxide perovskites by sulfur doping for electrocatalysis in rechargeable Zn-air batteries. *Chem Mater*, 2020, 32(8): 3439
- [128] Elumeeva K, Masa J, Sierau J, et al. Perovskite-based bifunctional electrocatalysts for oxygen evolution and oxygen reduction in alkaline electrolytes. *Electrochim Acta*, 2016, 208: 25
- [129] Elumeeva K, Masa J, Tietz F, et al. A simple approach towards high-performance perovskite-based bifunctional oxygen electrocatalysts. *ChemElectroChem*, 2016, 3(1): 138
- [130] Jung J I, Jeong H Y, Lee J S, et al. A bifunctional perovskite catalyst for oxygen reduction and evolution. *Angew Chem*, 2014, 126(18): 4670
- [131] Yuan R H, He Y, He W, et al. Bifunctional electrocatalytic activity of $\text{La}_{0.8}\text{Sr}_{0.2}\text{MnO}_3$ -based perovskite with the A-site deficiency for oxygen reduction and evolution reactions in alkaline media. *Appl Energy*, 2019, 251: 113406
- [132] Wang Z J, Zhang F, Jin C, et al. La_2O_3 -NCNTs hybrids *in-situ* derived from $\text{LaNi}_{0.9}\text{Fe}_{0.1}\text{O}_3$ -C composites as novel robust bifunctional oxygen electrocatalysts. *Carbon*, 2017, 115: 261
- [133] Bu Y F, Nam G, Kim S, et al. A tailored bifunctional electrocatalyst: Boosting oxygen reduction/evolution catalysis via electron transfer between N-doped graphene and perovskite oxides. *Small*, 2018, 14(48): 1802767
- [134] Hardin W G, Slanac D A, Wang X Q, et al. Highly active, nonprecious metal perovskite electrocatalysts for bifunctional metal-air battery electrodes. *J Phys Chem Lett*, 2013, 4(8): 1254
- [135] Yan L T, Lin Y E, Yu X E, et al. $\text{La}_{0.8}\text{Sr}_{0.2}\text{MnO}_3$ -based perovskite nanoparticles with the A-site deficiency as high performance bifunctional oxygen catalyst in alkaline solution. *ACS Appl Mater Interfaces*, 2017, 9(28): 23820
- [136] Peng S J, Han X P, Li L L, et al. Electronic and defective engineering of electrospun CaMnO_3 nanotubes for enhanced oxygen electrocatalysis in rechargeable zinc-air batteries. *Adv Energy Mater*, 2018, 8(22): 1800612
- [137] Li Z S, Lv L, Wang J S, et al. Engineering phosphorus-doped $\text{LaFeO}_{3-\delta}$ perovskite oxide as robust bifunctional oxygen electrocatalysts in alkaline solutions. *Nano Energy*, 2018, 47: 199
- [138] Majee R, Islam Q A, Bhattacharyya S. Surface charge modulation of perovskite oxides at the crystalline junction with layered double hydroxide for a durable rechargeable zinc-air battery. *ACS Appl Mater Interfaces*, 2019, 11(39): 35853